

**An Ensemble Circulation-Dependent Inflation Filter
in a Coupled GCM – Coping with Deep Ocean Biases,
Part I: Algorithm Design and Tuning**

S. Zhang* and A. Rosati

Geophysical Fluid Dynamics Laboratory, Princeton University

Princeton, NJ 08542, USA

(submitted to QJ)

* *Corresponding author address:* Shaoqing Zhang, GFDL/NOAA, Princeton University,
P.O. Box 308, Princeton, NJ 08542, USA. Email: Shaoqing.Zhang@noaa.gov Tel: (609)452-
6540 Fax: (609)987-5063

SUMMARY

An ensemble filter uses a Monte Carlo approach to estimating background error covariances instantaneously for extracting observational information, in which multiple model integrations run in parallel. This technique has shown great promise for atmospheric and oceanic data assimilation. The impacts of model biases on oceanic data assimilation (ODA) using coupled general circulation models (CGCMs) have been relatively unexplored. This study is the first in a sequence of studies using “biased” CGCMs to conduct ODA experiments, serving as a first step toward understanding the impacts of a fully-coupled GCM’s biases on ODA.

First, we design an “imperfect twin” experiment using two CGCMs that are biased with respect to each other, in which, simulated observations based on the 2005 Argo network are drawn from one CGCM and assimilated into the other. Using a standard ensemble filter, the assimilating imperfect model successfully recovers the upper-ocean temperature and salinity of the target model, but fails to converge in the deep ocean where a finite ensemble has difficulties to simulate the ocean’s intrinsic variability and model biases dominate. The inconsistency between the well-constrained upper ocean and poorly-constrained deep ocean generates spurious currents throughout the water column. Then, to cope with this problem, we introduce an ensemble circulation-dependent inflation filter (EcdiF) – which uses a pre-computed temporal variance to “inflate” the covariance wherever a small ensemble spread would otherwise make the model over-confident. The EcdiF greatly improves filtering performance, reducing global deep-ocean RMS errors by 30-40% for temperature, 40-50% for salinity, 70% for horizontal currents, and 50% for vertical velocity. The deep ocean improvements feed back on the upper ocean, resulting in an overall much better assimilation quality.

1 Introduction

Due to the lack of complete observations of climate variables and the existence of uncertainties in climate modeling, climate studies demand data assimilation to produce climate state estimates. The uncertainties in climate models come from inadequate measurements of natural and/or anthropogenic forcings, incomplete understanding on their radiative effects, as well as incomplete numerical implementation of physical processes, etc. These uncertainties can cause the model to drift away from the real world, called model bias. Generally, observations provide only some samples of climate variations in time and space, and are often sparse and noisy. To obtain more realistic climate evolution, data assimilation uses a climate model to extract information from observations. With advances of modeling and the enhancement of computational capability, data assimilation is playing an increasingly important role in climate studies.

Combining the needs of state estimation and forecast initialization, GFDL (Geophysical Fluid Dynamical Laboratory, NOAA) uses its second generation fully-coupled model (CM2) to implement climate data assimilation (Zhang et al. 2007). Based on *estimation theory* (Jazwinski, 1970), the GFDL coupled data assimilation (CDA) system directly solves for a temporally-evolving joint probability density function (joint-PDF) of climate states by combining the observational PDF and a prior PDF derived from the dynamically-coupled model. The ensemble filter first simulates the prior PDF by a Monte Carlo approach, i.e. launching a set of ensemble model integrations. Then states of each ensemble member are adjusted by observations using the first (expectation) and second (covariance) moments of the prior PDF through a linear regression. This kind of adjustment ensemble filtering approach (Anderson 2001; 2003) is able to maintain the features of higher-order moments of the prior PDF determined by the model dynamics at each analysis step. This ensemble system will eventually serve as an estimator of historical climate variations and support

predictions of future climate changes. The former is carried out by assimilating all observed data (presently only atmospheric and oceanic observations) into the model ensemble. The latter is realized by initializing the ensemble forecasts directly using the assimilation's atmospheric/oceanic/sea-ice/land ensemble states as initial conditions. In this way the ensemble forecasts have minimum initial shocks since all coupled components in each member stay in dynamical balances after experiencing a long time blending of data and model.

Two outstanding issues need to be addressed before one can estimate historical climate variations utilizing model and observed data: representation of climate observing system (e.g. Zhang et al. 2008) and impact of model bias (e.g. Segschneider et al. 2000; Balmaseda 2004; Vidard et al. 2005; Balmaseda et al. 2007). The latter is particularly challenging since neither defining model bias itself nor distinguishing the artifacts produced by model bias from the assimilation-generated variability is an explicitly feasible job in real data assimilation. To detect and understand the impact of the model bias in a CDA framework, two tracks – biased twin experiment research and quasi-operational real data assimilation – are performed in parallel at GFDL. The research track discovers issues in the presence of model bias and explores potential solutions that will be applied and eventually validated in the real data assimilation by evaluating their assimilation skill and forecast skill.

Pursuing the research track, this study first designs a twin biased ODA experiment using two coupled general circulation models (CGCMs) that are biased with respect to each other so that the model bias is unambiguously defined and the bias-generated artifacts in assimilation results are distinguished quantitatively. As a first step of long term efforts to understand the impacts of a fully-coupled GCM's biases on ODA, this study and its follow-up (Zhang and Rosati 2008) cope with a particular deep ocean bias issue when an ensemble filter is applied to estimate ocean states.

After the imperfect twin experiment using two biased CGCMs is introduced in section 2,

a general deep ocean bias problem induced by the differing ability of a finite (in both time integration length and sampling size) ensemble to represent the variability of upper and deep oceans is presented in section 3. The difficulties of a finite ensemble to represent the low-frequency deep ocean variability lead inconsistent data adjustments between the upper and deep oceans. The incoherent vertical structure can produce spurious velocities that degrade dramatically the assimilation’s performance. In section 4, an ensemble circulation-dependent inflation filter (EcdiF) is designed to improve the consistency between the upper and deep ocean data adjustments. Then EcdiF is evaluated by a 25-year parallel experiment in section 5. Conclusion and discussions are given in section 6.

2 Twin experiment of biased ODA

2.1 Two biased CGCMs at GFDL

Combining two different atmosphere models, AM2.0/LM2.0 and AM2.1/LM2.1, with the Fourth Version of Modular Ocean Model (MOM4) and the Sea Ice Simulator (SIS), GFDL has developed two fully-coupled general circulation models (CGCMs): CM2.0 and CM2.1. These two atmosphere models are based on different dynamical cores: B-grid finite-difference (Wyman 1996, GAMDT 2004) for AM2.0 and finite-volume (Lin 2004) for AM2.1 but have the same vertical (24 levels) and horizontal (2.5° longitude by 2° latitude) resolution, identical physical package and land model, with their own tuned parameters.

The MOM4 is configured with 50 vertical levels (22 levels of 10 m thickness each in the top 220 m), $1^\circ \times 1^\circ$ horizontal B-grid resolution telescoping to $1/3^\circ$ meridional spacing near the equator. The model has an explicit free surface with freshwater fluxes exchanged between the atmosphere and ocean. Parameterized physical processes include KPP vertical mixing, neutral physics, a spatially-dependent anisotropic viscosity, a shortwave radiative penetration depth that depends on a prescribed climatological ocean color. Isolation varies

diurnally and the wind stress at the ocean surface is computed using the velocity of the wind relative to surface currents. An efficient time-stepping scheme (Griffies 2005) is employed. More details can be found in Gnanadesikan et al. (2006). The SIS in the coupled model is a dynamical ice model with three vertical layers (one snow and two ice) and five ice-thickness categories. The elastic-viscous-plastic technique (Hunke and Dukowicz 1997) is used to calculate ice internal stresses, and the thermodynamics is a modified Semtner three-layer scheme (Winton 2000).

Detailed description for CM2.0 and CM2.1 and their major features for climate simulation can be found in Delworth et al. (2006) and Gnanadesikan et al. (2006). Here we only want to show a fundamental character – they are biased with respect to each other. Figures 1*ab* present the time averaged global mean temperature and salinity profiles over the last 25 years of the 140-year integrations of CM2.0 (solid-black) and CM2.1 (dashed-black). Both models use historical radiative forcings (the date of records are referred as the model calendar) and start from the same coupled initial conditions reset as 00UTC 1 January 1861 from previous study (Stoufer et al. 2004; also see Delworth et al. 2006). Figures 1*ab* show that over 1-6 km the mean bias of CM2.1 is 0.2°C colder and 0.01 PSU fresher vs. CM2.0.

2.2 Coupled ensemble filter

The probabilistic nature of the state evolution of a coupled model system is the basis of implementing coupled ensemble data assimilation. *filtering* theory (Jazwinski 1970) views the temporal evolution of coupled model states as a continuous stochastic dynamical process described by a vectorized stochastic differential equation as $d\mathbf{x}_t/dt = \mathbf{f}(\mathbf{x}_t, t) + \mathbf{G}(\mathbf{x}_t, t)\mathbf{w}_t$. Here, \mathbf{x}_t is an n -dimensional vector representing the coupled model state at time t (n is the size of the model state), \mathbf{f} is an n -dimensional vector function, \mathbf{w}_t is a white Gaussian process (uncorrelated in time) of dimension r with mean 0 and covariance matrix $\mathbf{S}(t)$ while

\mathbf{G} is an $n \times r$ matrix which defines the relation of the white Gaussian process and \mathbf{x}_t . The first and second terms of the right hand side in the equation represent respectively the contributions of deterministic modeling and uncertainties of modeling. While the dynamical model provides a background joint probability distribution (joint-PDF) for the states to be estimated, the Bayes' rule is used to combine the model-derived prior PDF and observational PDF to produce an analysed PDF. Ensemble-based filters use a Monte Carlo approach to simulate the prior PDF through finite-ensemble model integrations.

As described in Zhang et al. (2007), in the two-step local least square filtering implementation (Anderson 2003), at the first step, the i th ensemble member observational increment at the k th observational location, $\Delta y_{i,k}^o$, is computed [manipulated from Eqs. (2)-(5) in Zhang et al. 2007] as,

$$\Delta y_{i,k}^o = \frac{\bar{y}_k}{1 + \kappa^2(y_k, y_k^o)} + \frac{y_k^o}{1 + \kappa^{-2}(y_k, y_k^o)} + \frac{y_{i,k} - \bar{y}_k}{\sqrt{1 + \kappa^2(y_k, y_k^o)}} - y_{i,k}, \quad (1)$$

where the first two terms at the right hand side represent the shift of ensemble mean and the 3rd is the adjustment of ensemble spread, given a Gaussian observation $N(y_k^o, \sigma_k^o)$. y_k is the model's estimate for the observation y_k^o and an overbar represents the ensemble mean. $\kappa(y_k, y_k^o)$ is the ratio of standard deviations of the model ensemble estimated observational errors and real observational errors at the location k , i.e. σ_k/σ_k^o . At the second step, any oceanic state variable at grid-point j of the i th ensemble member, $x_{i,j}$, is adjusted [expanded from Eq. (6) in Zhang et al. 2007 to include the covariance localization] as,

$$\begin{aligned} \Delta x_{i,j} &= \Omega_{j,k} \frac{Cov(x_j, y_k)}{\sigma_{y_k}^2} \Delta y_{i,k}^o = \Omega_{j,k} r(x_j, y_k) \Delta y_{i,k}^o \\ &= \Omega_{j,k} \rho(x_j, y_k) \frac{\sigma_{x_j}}{\sigma_{y_k}} \Delta y_{i,k}^o = \Omega_{j,k} \rho(x_j, y_k) \kappa(x_j, y_k) \Delta y_{i,k}^o. \end{aligned} \quad (2)$$

Here $\rho(x_j, y_k)$ and $r(x_j, y_k)$ represent respectively the correlation coefficient and the linear regression coefficient between x_j and y_k . $\kappa(x_j, y_k)$ is the ratio of the ensemble-estimated standard deviations for x_j and y_k . Ω is the covariance localization function [$\Omega(a, d)$ in Zhang

et al. 2005] which is determined only by the distance between locations j, k . Since all error statistics evaluated by the model ensemble, $Cov(x_j, y_k)$, $\rho(x_j, y_k)$, σ_{y_k} , σ_{x_j} and $r(x_j, y_k)$, are the function of space and time, the background covariances used in the filtering are anisotropic and temporally-varying. For simplicity, Eq. (2) have dropped the common time subscript, t .

The ensemble filter outlined above has a few advantages for oceanic climate studies. First the filtering is a multi-variate analysis process based on the prior joint-PDF, which can maintain physical balances in oceanic circulations mostly. Second the temporally-evolving and spatially-anisotropic error covariances used at each analysis step allow the assimilation to capture features of local waves and the vertical variation of oceanic circulations. Third, the linear regression analysis adjusts only up to the second-order moments of the prior PDF but remains all higher-order moments, which sustains the nonlinearity in the long time evolution of oceanic circulations, for example, the bi-modal feature of the Atlantic thermohaline circulation (THC). Finally the assimilation within a coupled model system allows the coupled dynamics to impact the assimilation results through feedback processes between model components and therefore minimizes coupling shocks in initialization.

The *filtering* theory described above assumes both the dynamical model and the ensemble sampling of PDF are perfect. In practice, the dynamical model is biased and neither ensemble integration time nor ensemble size is infinity. A ‘finite’ ensemble always has a different representation for the different stochastic feature of oceanic circulations at different depth. Next, starting from a “twin” experiment using two CGCMs that are biased with respect to each other, we discuss the impact of deep ocean biases on the ensemble ODA.

2.3 Twin ensemble ODA experiment using two biased CGCMs

In order to examine the performance of the ensemble filtering ODA when the assimilation model is biased, we use one CGCM (CM2.0 in this study) to produce the “true” climate variation (called TRUTH hereafter) and corresponding “observations,” the other (CM2.1 in this study) to assimilate these “observations” for recovering TRUTH. We may call this as a biased assimilation “twin” experiment in which the “bias” is defined unambiguously and the bias-generated influences on assimilation results can be distinguished quantitatively. Same as in Zhang et al. (2008), the GFDL’s IPCC historical simulation produced by CM2.0 is set as the target (TRUTH) of assimilation. The other set of GFDL’s IPCC model integrations starting from the same initial conditions and using the same radiative forcings, but produced by CM2.1, is used as a free model control, called CTL, serving as a bottom line for assimilation evaluation: an assimilation must improve the oceanic (coupled) state estimates compared to CTL. The CTL simulation (by CM2.1) is also used to form ensemble initial conditions (ICs) for assimilation. The ensemble ICs are a set of yearly-separated atmospheric (including land) states combined with a common oceanic (including sea-ice) state. For example, the initial conditions of the 6-member ensemble (see section 3.3 for the justification on the ensemble size) that are used in this study are formed by combining the atmospheric and land states at 00 UTC 1 January of 1973-1978 and the oceanic and sea-ice states at 00 UTC 1 January 1976.

The observing system used in this study is the 21st-century Argo network. First the IPCC integration is re-run using the updated version of CM2.0 starting from 1 January 1976 up to 31 December 2000 to prepare the daily data of oceanic temperature and salinity. These model data are projected onto the 2005 Argo network through a tri-linear interpolation sampling process based on the Argo’s locations and depth, combined with a random noise superimposition (see Zhang et al. 2007; 2008).

Once oceanic “observations” (produced by CM2.0) and ensemble ICs are ready, using the ensemble filter described in section 2.2, the ‘biased’ ODA twin experiment is conducted. Except for the following two points new for this biased case, the ensemble filtering ODA algorithm [or called traditional ensemble filter, briefly ENSF) used here is the same as before (e.g. Zhang et al. 2007; 2008):

- 1) In order to reduce the assimilation shock, the daily adjustment of each adjusted variable is evenly distributed onto each time integration step instead of only being added once a day at each analysis step. In previous perfect model studies, the assimilation shock does not cause any serious problem but in this biased case, the large assimilation shock can significantly degrade the assimilation quality without doing so.
- 2) The adjustment of currents (U , V) based on cross-covariances between T , S and U , V is converted to acceleration and added into the time tendency of velocity update equations. By doing so, the barotropic and baroclinic modes are forwarded consistently as the model does, which minimizes possible computational modes induced by assimilation.

The coupled ensemble assimilation system is run for 25 years (from January 1976 to December 2000 of the model calendar). The TRUTH, ENSF and CTL global mean profiles are presented in Fig. 1*abc* and the ENSF-generated global RMS error reductions from CTL is presented in Fig. 2. From Figs. 1 and 2, two eye-striking phenomena are observed. 1) While the assimilation dramatically reduces temperature and salinity errors (Fig. 2*ab*), the errors of currents (Fig. 2*cd*) and vertical motions (Fig. 2*e*) are increasing beside the surface and bottom. 2) The error reduction of temperature and salinity has a strong depth dependence and the largest error reduction occurs around 0.5-2 km. Consistently, while the error reduction of temperature and salinity is dropped by the depth, the temperature and salinity

profiles in ENSF go back to CTL (Fig. 1*ab*). Currents and vertical motion diverge mostly from TRUTH (Fig. 1*c* and Fig. 2*cde*) as the error reduction of temperature and salinity decreases rapidly by depth (see Fig. 2*ab*).

Figure 2 also shows the temperature's error reduction is greater than the salinity's (the maximum value exceeds 70% for the former but only 55% for the latter), and the salinity error reduction can go deeper than the temperature's (the maximum value is located at the depth of 1-2 km for the former while 0.5-1 km for the latter). In addition, the temperature's error reduction of the top ocean above 500 m shows some short time scale features while the salinity's does not. Different time and vertical scales of assimilation error reduction of temperature and salinity imply that the salinity assimilation can be influenced by coupling feedback processes more than the temperature assimilation. For example, the small scale distribution of temperature error reduction near the surface indicates a direct observation impact of observed temperature profiles; the large time scale features of salinity error reduction reflect the dependency of the top ocean salinity on the atmospheric precipitation which comes from the atmosphere's responses to ODA-generated SSTs. The deeper assimilation influence for salinity may be associated with the response of the sea-ice processes to ODA, but the issue is beyond the scope of this study. The impact of sea-ice and land processes on ODA shall be discussed in separate studies.

Next, starting from analyses on difficulties of a finite ensemble to represent deep ocean's variability, we discuss the impact of deep ocean biases on ensemble ODA.

3 Impact of deep ocean biases on ensemble ODA

3.1 Difficulties of a finite ensemble to represent deep ocean’s variability

In order to show the differing ability of a finite ensemble to represent the upper and deep ocean variability, we first conduct a free ensemble model integration. The ensemble is initialized from yearly-separate atmospheric (including land) states combined with a common oceanic (including sea-ice) state (see section 2.3). Figure 3 presents the time mean ensemble spread of atmospheric and oceanic states over the last 10 years of a 25-year integration of CM2.1. Each solid line (different color) represents the departure of an individual ensemble member’s atmospheric/oceanic (upper/lower) temperature profile (left) or atmospheric specific humidity/oceanic salinity profile (right) from the ensemble mean; the dark dotted line in each panel shows the vertical variation of standard deviation of the corresponding ensemble spread computed by the 6-member ensemble. Due to strong internal variability (nonlinearity) of atmospheric flows, perturbations in both ICs and model-generated SSTs (as a consequence of ocean-atmosphere interaction) maintain the ensemble spread of atmospheric states which is nearly uniform vertically.

Different from the atmosphere, the ensemble spread of oceanic states reflects the sensitivity of ocean circulations to the surface forcings provided by the other coupled components (mainly by the atmosphere, wind stress and heat/water fluxes, for instance). Due to effects of mixing and convection, atmospheric disturbances can easily penetrate the upper ocean and alter thermocline where the largest oceanic spread is observed. In fact, the ensemble spread of oceanic temperature near the ocean surface has the same order of the magnitude as the atmospheric temperature’s ensemble spread in the lower troposphere. For a certain ensemble member while its temperature shows a nearly-continuous variation at the air-sea interface, the atmospheric specific humidity and the oceanic salinity appear basically located

at the opposite side of the ensemble mean at the bound of the atmosphere and ocean. This phenomenon reflects the fact that the atmospheric precipitation dominates the sea-surface salinity and they are negatively-correlated.

Figure 3 shows clearly below thermocline, the ensemble spread in deeper ocean reduces dramatically and compared to the model bias it becomes trivial by the depth very rapidly. This is because the oceanic circulations at different depth have a different response time scale to the surface forcings. In order to obtain an inter-ensemble variation in deeper ocean, a much longer ensemble spinup integration is required, and the deeper the ocean state goes the longer it requires to spin up the ensemble. Generally, the depth by which a significant ensemble spread can reach at a finite integration time is shallow in tropical oceans due to lacks of deep convection and deeper in middle or high latitudes (the North Atlantic deep convections may extend it toward deeper for instance). Although the deep ocean ensemble spread has a geographic dependence, compared to the model bias it becomes very small as the significant mixing effect vanishes.

It is worth to mention that as shown in upper panels of Fig. 3 except for moisture the internal variability of atmosphere does not significantly change with the height and therefore no serious incoherent vertical structure is observed in ensemble filtering atmospheric data assimilation.

3.2 Inconsistency of well-constrained upper ocean and poorly-constrained deep ocean in biased ensemble ODA

Figure 2 illustrates the challenge when a biased assimilation model is used to implement ODA: While the assimilation constrains the upper ocean temperature and salinity converging, oceanic velocities diverge. Checking the error distribution of velocities in ENSF we found the errors shown in Figs. 2*cde* mainly come from tropical oceans. Further checking

the analysis adjustment increments for temperature and salinity, we found the ENSF’s adjustment amount decreases very rapidly by depth below thermocline, especially in tropics, quickly becoming trivial compared to the model biases (see Figs. 1*de* as an example).

From the analyses of the last section, we learned that generally a finite ensemble can feasibly simulate the upper ocean’s variability which consists of ‘high’-frequency oscillations but it has difficulties to capture the low-frequency deep ocean variability - usually underestimated due to an insufficient ensemble spinup and sampling size. As the model ensemble spread is too small compared to the observational error (i.e. $\sigma_k \ll \sigma_k^o$), the observational increment [$\Delta y_{i,k}^o$ in Eq. (1)] goes to zero because $\kappa(y_k, y_k^o) \approx 0$. This is saying that the model becomes “over-confident” so that data are rejected ($\Delta x_{i,j} \approx 0$).

As we know, on geostrophy, pressure gradient is a dominant factor to determine ocean currents while upwelling/downwelling is induced by the divergence of currents. Recovering currents requires therefore higher-order accuracy than recovering temperature and salinity themselves using temperature and salinity observations while recovering upwelling/downwelling requires even higher-order accuracy than currents. Figs. 1*c* and 2*cde* show although the ENSF’s temperature and salinity are convergent over upper oceans the generated pressure gradient is not convergent yet.

The over-confidence of the model in deep ocean causes that as the upper ocean is converging to the data (TRUTH) the deep ocean stays with the biased model (CTL). Then ENSF constructs an incoherent vertical structure between the well-constrained upper ocean and the poorly-constrained deep ocean in a biased model. Note that pressure (watermass) is the vertical integral of density from surface to the current depth, which is computed by temperature and salinity, and pressure gradient is determined by watermass’s horizontal distribution at a certain depth. The incorrect watermass’s horizontal distributions caused by the incoherent vertical structure derive incorrect pressure gradients that lead to the spurious

velocities shown in Fig. 1c. The maximum spurious velocity zone corresponds to the layer at which the convergence rate of temperature and salinity is dramatically reduced (compare Figs. 2cd to Figs. 2ab). While the maximum spurious velocities appear between 500 - 2000 m, the velocities near surface and bottom appear slightly-improved. The slightly-improved velocities near surface can be explained by the ODA-improved mixing layer and the improved surface forcings, a consequence of the atmosphere’s responses to the ODA-generated SSTs. Near the bottom since barotropic and topographic effects increase and the dependency of velocities on the variability of internal circulations decreases, the errors of both currents and vertical motions are reduced.

The analyses above show that the underestimate of a finite ensemble spread to deep ocean variability is a primary reason that the traditional ensemble ODA produces spurious velocities.

3.3 Ensemble spinup vs. ensemble size in a finite ensemble

In implementing an ensemble data assimilation methodology, we always confront two practical issues: sampling size and assimilation ensemble spinup length. The former is constrained by the availability of computer resources and the latter is restricted not only by computer resources but also by data’s availability. Given that ocean’s subsurface data are only available in a limited time period (from a few years of Argo to a few decades of XBTs), the time scale of ensemble assimilation is always limited, in which the inter-ensemble variation for deep ocean has not well established yet through blending data and model dynamics. Although the problem posed in the last section is associated with ensemble size, results of tests using 6 and 24 ensemble members show that within an affordable scope, increasing the ensemble size does not change the essence of the problem.

How many members are appropriate in ensemble-based data assimilation is a very com-

plicated question for which there is no simple answer existing. For a certain ensemble assimilation algorithm, if a large ensemble size is used it is expected to increase the signal-to-noise ratio certainly, but it is strongly restricted by the availability of computation resources upon model's dimensions. For a comprehensive fully-coupled GCM like GFDL's CM2 which includes 4 coupled components, in which free dimensions exceed 20 million (basically $1^\circ \times 1^\circ$ ocean and $2.5^\circ \times 2^\circ$ atmosphere), even under a super-parallelization assimilation configuration (Zhang et al. 2007) computational resources still impose a strong constraint on the application of ensemble-based methodology. As the CGCM's resolution increases and physical processes become more complicated, the application of ensemble methodology will encounter more restrictions. Given the probabilistic nature of climate evolution and the uncertainties in both climate modeling and observations, implementing ensemble-based methodology for climate state estimation and prediction is an inevitable approach. We have long been engaged in designing and testing an ensemble-based algorithm that can work with a relatively small ensemble size.

In fact, even under a perfect model assumption, beside ensemble size, the assimilation's signal-to-noise ratio still depends on other 3 factors: 1) the temporal and spatial scales that assimilation model can resolve (i.e. the internal variability of assimilation model), 2) how to maintain the spread of the stochastic dynamical system (e.g. the representation of ensemble), and 3) the features of observations (e.g. the representation of observations). From Fig. 3, we learned that once an initial error occurs in the atmosphere or other coupled components, the strong internal variability of atmosphere and the ocean's responses to atmospheric forcings will eventually produce inter-ensemble variations of oceanic states through feedbacks. Experiments (e.g., Zhang et al. 2005; 2007) show that due to capturing the nature of oceanic states' uncertainty in the coupled model which consists of a coarse resolution OGCM, this kind of ensemble system is fairly reliable that it can work with a relatively small ensemble size. In addition, covariance filtering, or called covariance localization, and

observation smoothing techniques (Zhang et al. 2005; 2007) also help enhance the signal-to-noise ratio and maintain the system’s ensemble spread when a relatively small ensemble size is used. More test experiments in Zhang et al. (2007) also show that although a small ensemble size (6) is used, the coupled ensemble assimilation system is able to provide such a reliable T-S relationship that the multi-variate assimilation scheme (mainly utilizing T-S cross-covariances) dramatically enhances the assimilation’s signal-to-noise ratio relative to a univariate scheme. Considering the essence of the problem addressed in this study (mainly caused by the limited ensemble assimilation length) and the character of the coupled model ensemble as well as the constraint of computational resources, we continuously use 6 members in this study. The same ensemble configuration also makes it convenient to compare the biased ODA results with the previous perfect model ODA results.

4 EcdiF – An ensemble circulation-dependent inflation filter

4.1 Correlation vs. standard deviation in filtering

The problem posed in section 3.2 is a product of combining model biases with the poor representation of a finite ensemble to the low-frequency deep ocean variability.

Background error covariance is a key parameter in implementing data assimilation (used in the linear regression process of ensemble filters, for instance). For example, as the adjusted variable in model states has the same physical dimension as observed variable, analysis process uses auto-covariance to distribute an observational increment onto adjacent model grids. While observations and the adjusted variables have different physical dimension, cross-covariance is used to transform the signal of an observational increment from one physical space to another. As the second moment of the background joint-PDF, covariance reflects the relationship of disturbance “energy” variations of two variables with the same

(for auto-covariance) or different (for cross-covariance) physical dimension, which consists of correlation and standard deviations of these two variables. As discussed in Zhang and Anderson (2003), generally, standard deviation, σ , (or variance, σ^2) represents the magnitude of disturbance “energy” varying of a variable at a certain location while correlation (ρ) reflects the relationship of fluid’s motion status (phase-in or phase-out in waves, for instance) of either the same physical variable at different spatial locations (auto-correlation) or different variables at the same/different spatial locations (cross-correlation). Equations (1) and (2) show the standard deviation and correlation evaluated by model ensemble play a different role in the filtering algorithm. The standard deviation of the model ensemble spread determines the amount of observational increment [$\Delta y_{i,k}^o$ in Eq. (1)] and it therefore controls the strength of data constraint while correlation mainly governs the sign (direction) of the data projection in the linear regression.

Figure 4 gives an example of how standard deviation (σ , top) and correlation (ρ , bottom) evaluated by a long time series of T, S anomalies in CM2.0 (left, denoted by σ_0, ρ_0) and the time mean of 6-member ensemble spread in CM2.1 (right, denoted by $[\sigma_t], [\rho_t]$) are different. Two fundamental characters are observed in Fig. 4: 1) $[\sigma_t]$ exhibits similar geographical patterns as σ_0 , which are associated with local circulation systems, but $[\sigma_t]$ is smaller than σ_0 by one order of magnitude over top ocean and more than one order below 1 km; 2) ρ_0 and $[\rho_t]$ have different structures. On one hand, as pointed by Zhang and Anderson (2003), a finite ensemble provides a reasonable estimate for the correlation structure that represents mostly the physical balance required by the assimilation model dynamics at the analysis snapshot. On the other hand, estimating standard deviation requires a much refined ensemble, i.e. an aggressively prolonged ensemble assimilation spinup in this biased ODA case, which is extremely restricted by the availability of observations and computational resources.

Next, based on covariance inflation theory of *filtering* (Chapter 8, Jazwinski 1970), a

new algorithm, called ensemble circulation-dependent inflation filter (EcdiF) is designed to answer: 1) How to strengthen deep ocean data constraints without damaging physical balances required by model dynamics? 2) Once deep ocean adjustments becomes significant, how to extend the adjustments produced at the bottom of observed profiles to deeper to minimize the discontinuities of data adjustments?

4.2 Algorithm design of EcdiF

Covariance inflation is a common practical approach (Anderson 1999; 2007; Zhang and Anderson 2003) to improve the performance of ensemble filters, which was born as a part of *filtering* theory (e.g. Chapter 8, Jazwinski 1970). However, the application of the theory requires a very cautious examination of the geo-fluid system to which it is applied. First given the character of oceanic circulation's variability at different depth shown by Fig. 3, the method applied to simple models [with a globally-uniform inflation coefficient such as Anderson (1999; 2007) and Zhang and Anderson (2003)] is not applicable for the comprehensive model system. Second, as described before, for a non-eddy-resolving ocean model which has small internal variability, directly inflating the ensemble which comes from the dynamical responses to perturbed surface forcings is inappropriate. What follows outlines a specific application of covariance inflation theory according to the features of the current GFDL's coupled ensemble system.

The new algorithm uses the pre-computed standard deviations (e.g. Fig. 4a) from a long time series of existing oceanic state's anomalies (CM2.0 model simulations in this case) to inflate the ensemble-evaluated deep ocean's covariance. This kind of inflation is performed according to what the variability of climatological circulations allows. The standard deviations computed by a long time series of oceanic state's anomalies reflect the deep ocean's variability of the ocean model responding to surface forcings over one hundred years (1861-

2000). The use of monthly anomalies also greatly increases the sample size (equivalent to using 300 ensemble members) for computing the standard deviation of deep ocean's circulations. In addition, in order to mostly sustain the temporally-evolving nature of upper ocean's covariances and model's physical balances, the new algorithm consists of an optimal combination of un-inflated and inflated adjustments. Then, the new filtering equation can be written as

$$\Delta x_{i,j} = \begin{cases} \Omega_{j,k} \rho_t(x_j, y_k) \kappa_t(x_j, y_k) \Delta y_{i,k,t}^o, & Z \leq Z_0 \\ \Omega_{j,k} \rho_t(x_j, y_k) \left[\frac{\kappa_t(x_j, y_k)}{\kappa_t(x_j, y_k) + \kappa_0(x_j, y_k)} \Delta y_{i,k,t}^o + \frac{\kappa_0(x_j, y_k)}{\kappa_t(x_j, y_k) + \kappa_0(x_j, y_k)} \Delta y_{i,k,0}^o \right], & Z > Z_0 \end{cases} \quad (3)$$

and

$$\Omega_{j,k} = \begin{cases} \Omega(a^h, d_{j,k}^h) \Omega(a^v, d_{j,k}^v), & D^o \neq D_{bottom}^o \text{ or } D^o = D_{bottom}^o \text{ but } Z \leq D_{bottom}^o \\ \Omega(a^h, d_{j,k}^h) \Omega(a_b^v, d_{j,k}^v), & D^o = D_{bottom}^o \text{ and } Z > D_{bottom}^o \end{cases} \quad (4)$$

Here $\kappa_0(x_j, y_k)$ is the ratio of the values of σ_0 for x_j and y_k and $\Delta y_{i,k,0}^o$ is the observational increment computed by σ_0 [the prior background standard deviation, σ_k , in Eq. (1) is replaced by the corresponding $\sigma_{k,0}$]. a^h and a^v are the e-folding horizontal and vertical scales in the covariance localization function respectively, and $d_{j,k}^h$ and $d_{j,k}^v$ is the horizontal and vertical distance between x_j and y_k . D^o and D_{bottom}^o represent respectively the current observation depth and the depth at the bottom of an observed profile, and Z is the vertical coordinate. Two tunable parameters, Z_0 , the threshold depth of using σ_0 , and a_b^v that controls the impact depth to which the adjustment from the bottom of an observed profile is extended, are introduced into the algorithm to address the 2rd question posed at the end of section 4.1.

Parameter Z_0 defines the starting depth to apply σ_0 , which will be tuned and study in the next section. Although Z_0 could be a function of geographic locations it is set as a global uniform value in this study as a first version due to the application of the weighting combination technique in Eq. (3). Obviously, if Z_0 is set to be greater than the bottom of the model ocean (5316 m in MOM4), this algorithm is degraded to the traditional ensemble filter.

The application of parameter a_b^v is a little complicated. In ENSF, 4 cases are distinguished: case-1 – if D_{bottom}^o is less than 500 m it is set as the same as a^v (2 model levels below and above the current observation depth); case-2 – if D_{bottom}^o is between 500 m and 1 km it is set as 1 more model levels than a^v ; case-3 – if D_{bottom}^o is between 1 km and 2 km it is set as 2 more model levels than a^v ; case-4 – if D_{bottom}^o is 2 km or below it is set as 4 more model levels than a^v . Since most of Argo profiles go to 2 km, only case-3 and case-4 apply to the Argo network ($a_b^v \approx 1000$ m at $D_{bottom}^o = 2$ km, for instance). Generally due to the underestimate of ensemble variance at deep ocean, the use of these a_b^v values only make a refined ramp for the adjustment from the bottom of observed profiles and increasing the a_b^v value cannot make an efficient extension for bottom adjustments. In the new algorithm since the deep ocean adjustment magnitude can be enlarged by $\kappa_0(x_j, y_k)$, a_b^v becomes an important parameter for enhancing the assimilation quality.

An example of the relative amplitude of the time mean of $r_{tt}(T, S)$ computed using $\kappa_t(T, S)$ and $\rho_t(T, S)$ (top) and $r_{t0}(T, S)$ computed using $\kappa_0(T, S)$ and $\rho_t(T, S)$ (middle) is given in Fig. 5. At the tropical Pacific, the signals in the time mean of $r_{tt}(T, S)$ appear very weak below 500 m, while the signals in the time mean of $r_{t0}(T, S)$ are much stronger and can extend up to 3 km. As compensation, the new algorithm may let the linear regression coefficients used in filtering take account the strength of $r_{t0}(T, S)$ below 500 m, as shown by their average, denoted as $r_t^{EcdiF}(T, S)$ (panel c). On the contrary, in the North Atlantic (not shown), due to the existence of the strong variability of gyres, the time mean of $r_{tt}(T, S)$ shows stronger signals in the regions of subtropical and subpolar gyres than the $r_{t0}(T, S)$ does. Under this circumstance, their average turns out to be a relaxed version of $r_{tt}(T, S)$ using a relatively small $\kappa_0(T, S)$.

In this twin experiment study, σ_0 used to inflate the filtering adjustment is computed from the time series of CM2.0 model simulations (TRUTH). In the application to assimilating real

data, starting from a climatology estimate, σ_0 can be refined by accumulated assimilation products. This way may further increase the impact of observations in real data assimilation.

4.3 Tuning of EcdiF

Tuning parameters in this ensemble coupled system for climate time scales requires huge computational cost. In order to increase the efficiency of parameter tuning, tests are performed with three different time scales. First, 5-day tests with each time step output are compared to choose the candidates of parameter values that produces the self-consistent good results, especially not creating any instanteneous upwelling/downweling. Then 1-month tests with daily output are compared cross the chosen candidates to ensure the parameter value to be optimal within one month. Finally the optimal paramter value is set into a long run (at least one year) to ensure it works for long term climate estimate.

Generally, a small value for Z_0 means less confidence on σ_t so that even for upper ocean, the assimilation adjustment is modified by σ_0 . For example, if $Z_0 = 0$ the application of Eq. (4) will even modify the adjustment of the mixed layer in ensemble filtering by the temporal standard deviation of anomalies, which may be necessary when a really small ensemble size is used. On the contrary, the use of a large Z_0 will remain the temporally-evolving character of regression coefficients in filtering mostly, which may happen when the ensemble assimilation has been performed for a long time and a large ensemble is used. The a_b^v value reflects the confidence of both the assimilation adjustment amount at the bottom of the observed profiles and the ensemble-evaluated correlation at deep ocean.

Three Z_0 values – 0, 500m, 1 km and three a_b^v values – $a_b^{v,ENSF}$, $2a_b^{v,ENSF}$ and $4a_b^{v,ENSF}$ participate in the EcdiF tuning in this study. Each value of Z_0 and a_b^v is first tested in a 5-day length. Results show that, generally, for Z_0 , a smaller value produces better assimilation quality, and for a_b^v , a larger value produces better assimilation quality. Then some cross test

experiments combining Z_0 and a_b^v are carried out in a one-month length. In particular, for the Argo network used in this study in which most of profiles end at 2 km, the following values of a_b^v appeared in bracket are examples when $D_{bottom}^o = 2$ km applied to case-4 described in section 4.2. The following 5 experiments are compared and discussed in details:

EcdiF₀ – using $Z_0 = 1$ km and $a_b^v = a_b^{v,ENSF}$ (≈ 1 km),

EcdiF₁ – using $Z_0 = 1$ km and $a_b^v = 2a_b^{v,ENSF}$ (≈ 2 km),

EcdiF₂ – using $Z_0 = 500$ m and $a_b^v = 2a_b^{v,ENSF}$,

EcdiF₃ – using $Z_0 = 500$ m and $a_b^v = 4a_b^{v,ENSF}$ (≈ 4 km), and

EcdiF₄ – using $Z_0 = 0$ and $a_b^v = 4a_b^{v,ENSF}$.

Figure 6 gives examples of covariance vertical ramp functions $\Omega(a_b^v, d^v)$ when $a_b^v = a_b^{v,ENSF}$ (≈ 1 km, dotted), $2a_b^{v,ENSF}$ (≈ 2 km, dashed) and $4a_b^{v,ENSF}$ (≈ 4 km, solid) as $D_{bottom}^o = 2$ km. As $a_b^v = 4a_b^{v,ENSF}$ (≈ 4 km at $D_{bottom}^o = 2$ km), the e-folding depth exceeds the the bottom of the model ocean, which means that the adjustment amount at the bottom of most Argo profiles is extended up to full ocean depth with the ramp function plotted by the solid curve in Fig. 6.

The RMS errors of oceanic temperature (left) and salinity (right) at different layers produced by these test experiments are shown in Fig. 7 in which errors of the model control (CTL) and traditional ensemble filter (ENSF) are plotted by black-dotted and black-solid lines as references. From top (*ab* for top 500 m) and upper-middle (*cd* for 500-1000 m) panels, we find that EcdiF consistently strengthens data constraint when Z_0 change its value from 1 km, 500 m to 0. For top 500 m, only the RMS error of EcdiF₄, in which the inflation starts at the surface, gets dramatically reduced from ENSF's ($\approx 10\%/12\%$ for temperature/salinity) while other 4 experiments – EcdiF_{0,1,2,3} that do not inflate until 500 m – only reduced their

errors no more than 4%. For 500-1000 m, three of experiments – EcdiF_{2,3,4} in which all adjustment below 500 m are inflated – reduce their errors by 20% and 25% for temperature and salinity respectively. From top (*ab*) and upper-middle (*cd*) panels, it is also observed that upper ocean states can be corrected slightly due to a substantial correction for deep ocean states, especially for salinity. For example, although the top 500 m filtering adjustments in EcdiF_{2,3} are the same as in EcdiF_{0,1} the top 500 m RMS errors of EcdiF_{2,3} are noticeably smaller than the errors of EcdiF_{0,1} because more substantial corrections are made in EcdiF_{2,3} than in EcdiF_{0,1} below 500 m. Lower-middle (*ef*) and bottom (*gh*) panels show that the use of a proper a_b^v value in EcdiF is very important to get sufficient corrections for ocean states below 1 km. Both doubling (EcdiF_{1,2}) and quadrupling (EcdiF_{3,4}) the a_b^v value from $a_b^{v,ENSF}$ make the same error reduction for the 1-2 km layer (10% and 25% for temperature and salinity) but the latter makes almost double more error reduction than the former does for the layer below 2 km. This means that it's very important to coherently extend the adjustments produced at the bottom of observed profiles toward deeper for estimate the deep ocean states.

Another interesting phenomenon is the interaction of circulations among different layers. All EcdiF_{0,1,2,3} experiments do not inflate the filtering correction above 500 m. It is however clear that the top 500 m errors of EcdiF_{2,3} (blue-dashed and blue-dotted-dashed lines in panels *ab* of Fig. 7) are smaller than the errors of EcdiF_{0,1} (thin-dashed and thick-dotted lines in panels *ab*). It is the improvement of circulations below 500 m in EcdiF_{2,3} that causes the improvement of their top ocean circulations. Comparing the assimilation errors of EcdiF₃ (blue-dotted-dashed lines) and EcdiF₄ (red-solid lines), we find that the improvement of top 500 m circulations in EcdiF₄ does not have much impact on the circulations of the 500 m to 2 km layer but improving the circulations below 2 km. Due to JEBAR (Joint Effect of Baroclinicity and Bottom Relief, see Sarkisyan and Ivanov 1971; Mellor et al. 1982; Myers et al. 1996) top ocean barotropic modes may have direct influence on bottom ocean within

the one-month time scale. We shall keep eyes on this phenomenon in the future assimilation experiments to obtain more detailed understanding.

It is also interesting to see how EcdiF changes the correction distribution in filtering. Fig. 8 shows the horizontal distribution of the top 500 m (averaged) temperature (left, *ac*) and salinity (right, *bd*) corrections without (in EcdiF₃) (top, *ab*) or with (in EcdiF₄) inflation for top 500 m ocean. With the same positive/negative correction patterns as EcdiF₃, EcdiF₄ increases the correction magnitude. In the Pacific and Atlantic Oceans, the major correction-strengthened regions, by order, are subpolar gyres, subtropical gyres and the equatorial current system. The correction-strengthening is also observed in the Southern and Indian Oceans. Consistent with the RMS error reduction, the salinity correction is strengthened more than the temperature correction. This suggests that it is more difficult using ensemble approach to estimate the salinity standard deviation than to estimate the temperature standard deviation. The vertical distribution of temperature and salinity corrections on the y-z plane (not shown) shows some discontinuities of filtering corrections at 1 km or 500 m in EcdiF_{1,3} although the application of the weighting combination technique [Eq. (3)] in EcdiF. Due to the application of 0 and $4a_b^{v,ENSF}$ for Z_0 and a_b^v , EcdiF₄ produces very smooth corrections and the correction amount around 2 km (bottom of Argo) is consistently extended to deeper ocean, so that it makes the best assimilation quality as shown in Fig. 7. Finally, we examine the RMS errors of currents and vertical motions to see if the inflated filtering corrections in 5 EcdiF experiments introduce extra imbalance into oceanic circulations. Overall speaking, all 5 EcdiF experiments do not produce any extra imbalance in the circulations above 2 km. In fact, due to the improvement of vertical consistency of filtering corrections (see the blue lines in Fig. 1*de* as an examples), currents and vertical motions above 1 km in all EcdiF experiments have been improved after around 10 days for spinup. As discussed in section 3.2, as depth increases, the accuracy of pressure's horizontal gradient decreases due to the accumulation of assimilation errors in the vertical integral of

water’s density. Then longer assimilation is required in order to reduce the errors of currents and vertical motions in deeper ocean.

5 Tests in a 25-year long run

This section expands the validation of EcdiF initialized in section 4.3 in a longer assimilation run, still focusing on global scale statistics. The impact of EcdiF on oceanic climate detection including the oceanic heat and salt transport and the variability of heat content, El Niño-Southern Oscillation (ENSO) and the North Atlantic (NA) meridional overturning circulation (MOC) etc., will be examined in details in Part II (Zhang and Rosati 2008).

For efficiently using the computational resources in the long run test, EcdiF₀ is run for 1 year (1976), EcdiF₂ for 3 years (77-79), EcdiF₃ for 6 years (80-85) and then EcdiF₄ for the rest up to 2000. The RMS error reductions on 5 oceanic state variables produced by this EcdiF long run from ENSF are shown in Fig. 9. Figure 9 shows that EcdiF has more potential to improve the assimilation quality for salinity than for temperature, but the salinity assimilation quality appears more sensitive to the values of parameters Z_0 and a_b^v . Throughout the whole 25-year test period, EcdiF makes almost the same level temperature error reduction (the maximum goes to 30-40% between 2-3 km) with these 4 sets of parameter values (panel *a*). A small value for a_b^v cannot make the inflated filtering adjustment improve the salinity estimate deeper than 4 km as the EcdiF reduces the salinity error up to 40-50% above 4 km (maximum error reduction appears between 1-2 km) (panel *b*). When a 4 km a_b^v value is used, the EcdiF starts to improve the salinity estimate below 4 km. Overall, since EcdiF improves the vertical consistency of assimilation convergence so as to improve the estimate of water mass, the assimilation quality of currents and vertical motions has been improved dramatically above 4.5 km – the maximum error reduction goes up to 70% for currents and 50% for vertical motions between 1-2 km. It’s natural that the smallest

improvement on velocities is occurred at the bottom.

The horizontal distribution of temperature (left, *ac*) and salinity (right, *bd*) assimilation errors in ENSF (top, *ab*) and EcdiF (middle, *cd*) is shown in Figs. 10 (for top 4 km average). Generally, EcdiF reduces dramatically assimilation errors of temperature/salinity in the regions where the horizontal gradient of temperature/salinity is relatively small (over tropics and subtropics, for instance) (see the mean temperature and salinity in Figs. 10*ef*) This is because as the horizontal gradient of temperature/salinity is small, the circulations have strong low-frequency features so that a relatively short time ensemble integration has more difficulty to represent their variance. Over the regions where the temperature and salinity gradient is strong (e.g. the North Pacific and Atlantic subpolar gyres, the Antarctic circumpolar circulation) EcdiF has more difficulty to reduce the assimilation errors. In particular, over the region of the northwest of Atlantic Ocean connecting to the Labrador Sea, the top 2 km averaged temperature and salinity (especially for temperature) assimilation errors appear worse in EcdiF than in ENSF. This must be associated with the NA MOC's structure and its variability which may require a refined adjustment inflation and extension scale. This issue will be further examined and discussed in follow-up study. Consistent with the substantial improvement on the estimates of tropical temperature and salinity, the vertical section of u-component and vertical motion errors (Fig. 11) shows that the errors of currents and vertical motions of ENSF below 500 m due to the vertical inconsistency of filtering convergence are mostly eliminated in Pacific and Indian Oceans. The improvement of tropical currents and vertical motions in the Atlantic Ocean is relatively smaller than other two basins, and again, this will be explored more in follow-up studies.

6 Conclusions and discussions

An ensemble filter uses ensemble model integrations to instantaneously evaluate background error covariances and the temporally-evolving error statistics is good for capturing upper ocean variability in oceanic data assimilation. The stochastic character of oceanic circulations varies from location to location, especially with depth. The variance of the tropical ocean temperature, salinity and currents is mostly concentrated above 500 m, and the ensemble spread decreases dramatically below the thermocline. The subtropical and subpolar gyres can extend the spread much deeper in extratropics. Generally the deeper circulations are dominated by lower-frequency fluctuations, making it difficult for an ensemble filter to smoothly capture the signals of interest – in the face of infrequent observations and model biases – when both ensemble integration length and ensemble size are limited.

To examine impacts of model biases on oceanic data assimilation with the ensemble filter, we have described an “imperfect twin” experiment in which one model – the GFDL CM2.0 CGCM – is designated to produce the “truth,” and the other model – the GFDL CM2.1 CGCM – is used to assimilate simulated observations that sample the truth according to the 2005 Argo network. The results show that using a traditional ensemble filter with a biased model can lead to vertical inconsistency in the analysis solution, as the upper ocean is assimilated more effectively than the deep ocean. The vertical inconsistency between the well-assimilated upper and poorly-assimilated deep oceans generates spurious currents and vertical velocities throughout the water column.

An ensemble circulation-dependent inflation filter (EcdiF) has been designed to improve the vertical consistency of ensemble filtering oceanic data assimilation. The EcdiF retains an ensemble-estimated correlation structure to maintain the physical balance required by model dynamics, but incorporates an anomaly’s variance – estimated *a priori* from a long time series of oceanic states – to inflate the covariance where the ensemble spread would

otherwise be too small.

A 25-year test shows that compared to the traditional ensemble filter, the EcdiF improves the assimilation quality for both temperature and salinity throughout the ocean, especially in the tropics and subtropics. The EcdiF substantially improves the vertical consistency of the ODA, with deep-ocean (1-4 km depth) global RMS errors reduced by up to 30-40% for temperature and 40-50% for salinity. This in turn improves the oceanic currents above 4.5 km, reducing global RMS errors by up to 70% for horizontal currents and 50% for vertical velocities. That the equatorial undercurrent and upwelling are improved offers hope for improved initialization of ENSO forecasts. And the improved deep ocean solution is encouraging for estimating – and possibly predicting – decadal and multi-decadal fluctuations in the North Atlantic meridional overturning circulation.

Despite these many improvements, several challenges remain. Over the northwest Atlantic and Labrador Sea, and near the ocean bottom, the temperature and salinity assimilation errors remain, as discussed in follow-up study (Zhang and Rosati 2008) on local tuning of EcdiF's parameters to sustain the north Atlantic deep convection. Handling bias issues (Bell et al. 2004; Dee 2005; Balmaseda et al. 2007) and pursuing better balanced oceanic analyses (e.g., Gerrit et al. 2002) remain a topic of active research and development for the GFDL's climate estimation and prediction. For example, reducing biases in the surface forcings, through better atmospheric data assimilation using 24-member ensemble CDA, has improved the coupled initial conditions of GFDL's ENSO forecasts as measured by the model ENSO forecast skill (to be reported in a future study). Furthermore, implementing the EcdiF as a coupled reanalysis with real data is improving the oceanic state estimates of the deep oceans and extratropics, which is promising for longer-term forecasts and projections on decadal-to-century time scales. A multi-model ensemble assimilation and prediction system, which incorporates multiple CGCMs into the ensemble filter is currently being tested at

GFDL and shows promise for reducing assimilation biases.

ACKNOWLEDGEMENT

Special thanks go to Drs. Andrew Wittenberg and Matthew J. Harrison for their thorough examination on the earlier version of this manuscript, which is very helpful to improve the manuscript. The authors also like to thank Drs. Qian Song and Tony Gordon for their comments on the earlier version. Thanks go to Drs. Guijun Han and You-Soon Chang for their suggestions in processing observation data during their visiting at GFDL. The authors thank two anonymous reviewers for their thorough examination and comments that are very useful for improving the manuscript.

REFERENCES

- Anderson, J. L., 2007: An adaptive covariance inflation error correction algorithm for ensemble filters. *Tellus*, **59A**, 210–224.
- Anderson, J. L., 2003: A local least squares framework for ensemble filtering. *Mon. Wea. Rev.*, **131**, 634–642.
- Anderson, J. L., 2001: An ensemble adjustment Kalman filter for data assimilation. *Mon. Wea. Rev.*, **129**, 2884–2903.
- Anderson, J. L., 1999: A Monte Carlo implementation of the nonlinear filtering problem to produce ensemble assimilations and forecasts. *Mon. Wea. Rev.*, **127**, 2741–2758.
- Balmaseda, M. A., 2004: Ocean data assimilation for seasonal forecasts. *ECMWF Seminar Proceedings*. Seminar on Recent developments in data assimilation for atmosphere and ocean, 8-12 September 2003, 301 – 326.
- Balmaseda, M. A., D. Dee, A. Vidard and D. T. Anderson, 2007: A multivariate treatment of bias for sequential data assimilation: Application to the tropical oceans. *Quart. J. Roy. Meteor. Soc.*, **133**, 167–179.
- Dee, D. P. and A. M. D. Silva, 1998: Data assimilation in the presence of forecast bias. *Quart. J. Roy. Meteor. Soc.*, **124**, 269–295.
- Dee, D. P., 2005: Bias and data assimilation. *Quart. J. Roy. Meteor. Soc.*, **131**, 3323–3343.
- Delworth, T. L., A. Rosati, Ronald J. Stouffer, Keith W. Dixon, John Dunne, Kirsten L. Findell, Paul Ginoux, Anand Gnanadesikan, C. T. Gordon, Stephen M. Griffies, Rich Gudgel, Matthew J. Harrison, Isaac M. Held, Richard S. Hemler, Larry W. Horowitz, Stephen A. Klein, Thomas R. Knutson, Shian-Jiann Lin, V. Ramaswamy, M. Daniel Schwarzkopf, Joseph J. Sirutis, Michael J. Spelman, William F. Stern, Michael Winton, Andrew T. Wittenberg, Bruce Wyman, A. J. Broccoli, R. J. S. V. Balaji, Joellen Russell,

- Rong Zhang, John A. Beesley, Jian Lu, William F. Cooke, Jeffrey W. Durachta, Amy R. Langenhorst, Hyun-Chul Lee, Fanrong Zeng, K. A. Dunne, P. C. D. Milly, Paul J. Kushner, Sergey L. Malyshev and Elena Shevliakova, 2006: GFDL CM2 global coupled climate models, Part I: Formulation and simulation characteristics. *J. Climate*, **19(5)**, 643–674.
- Gerrit, B., M. A. Balmaseda, F. Vossepoel, G. J. Van Oldenborgh and P. J. Van Leeuwen, 2002: Balanced ocean-data assimilation near the equator. *J. Phys. Oceanogr.*, **32**, 2509–2519.
- Gnanadesikan, A., Keith W. Dixon, Stephen M. Griffies, Thomas L. Delworth, Matthew J. Harrison, Isaac M. Held, William J. Hurlin, Ronald C. Pacanowski, Anthony Rosati, Bonita L. Samuels, Michael J. Spelman, Ronald J. Stouffer, Michael Winton, Andrew T. Wittenberg, John P. Dunne, V. Balaji, Marcelo Barreiro, Joellen Russell, Qian Song, Colm O. Sweeney, Rong Zhang, J. Anthony Beesley, Gabriel Vecchi, William F. Cooke, Hyun-Chul Lee, Zhi Liang, Giang Nong, Fanrong Zeng, Rudiger Gerdes, 2006: GFDL CM2 global coupled climate models, Part II: The baseline ocean simulation. *J. Climate.*, **19(5)**, 675–697.
- Griffies, S. M., M. J. Harrison, R. C. Pacanowski and A. Rosati, 2003: A Technical Guide to MOM4. *GFDL Ocean Group Technical Report*, No. 5, Princeton, NJ 08542, NOAA/Geophysical Fluid Dynamics Laboratory, 295 pp.
- Griffies, S. M. and R. W. Hallberg, 2000: Biharmonic friction with a Smagorinsky-like viscosity for use in large-scale eddy-permitting ocean models. *Mon. Wea. Rev.*, **128**, 2935–2946.
- Griffies, S. M., 2005: Some ocean model fundamentals. In: *Ocean Weather Forecasting: an integrated view of Oceanography*. E. P. Chassignet and J. Verron, eds., Berlin, Germany: Springer, 19–74.

- Hunke, E. C., and J. K. Dukowicz, 1997: An elastic-viscous-plastic model for sea ice dynamics. *J. Phys. Oceanogr.*, **27**, 1849–1867.
- Jazwinski, A. H., 1970: *Stochastic Processes and Filtering Theory*. Academic Press, New York, 376pp.
- Lin, S-J., 2004: A "vertically Lagrangian" finite-volume dynamical core for global models. *Mon. Wea. Rev.*, **132**, 2293–2307.
- Mellor, G., C. R. Mechoso and E. Keto, 1982: A diagnostic calculation of the general circulation of the Atlantic Ocean. *Deep-Sea Research*, **Vol. 29, No. 10A**, 1171–1192.
- Mellor, G. and T. Ezer, 1991: A Gulf Stream model and an altimetry assimilation scheme. *J. Geophys. Res.*, **96**, 8779–8795.
- Myers, P. G., A. F. Fanning and A. J. Weaver, 1996: JEBAR, bottom pressure torque, and Gulf Stream separation. *J. of Physical Oceanography*, **26**, 671–683.
- Sarkisyan, A. S, and V. F. Ivanov, 1971: Joint effect of baroclinicity and bottom relief as an important factor in the dynamics of sea currents. *Izv., Atmospheric and Oceanic Physics*, **Vol. 7, No. 2**, 172–188.
- Segschneider, J. M. A. Balmaseda, D. L. T. Anderson, 2000: Anomalous temperature and salinity variations in the tropical Atlantic: possible causes and implications for the use of altimeter data. *Geophys. Res. Lett.*, **17(15)**: 2281.
- Sarkisyan, A. S, and V. F. Ivanov, 1971: Joint effect of baroclinicity and bottom relief as an important factor in the dynamics of sea currents. *Izv., Atmospheric and Oceanic Physics*, **Vol. 7, No. 2**, 172–188.
- Vialard, J., F. Vitart, M. A. Balmaseda, T. N. Stockdale and D. L. T. Anderson, 2005: An ensemble generation method for seasonal forecasting with an ocean-atmosphere coupled model. *Mon. Wea. Rev.*, **131**, 1379–1395.

- Winton, M., 2000: A reformulated three-layer sea ice model. *J. Atmos. Ocean. Tech.*, **17**, 525–531.
- Zhang, S. and J. L. Anderson, 2003: Impact of spatially and temporally varying estimates of error covariance on assimilation in a simple atmospheric model. *Tellus*, **55A**, 126–147.
- Zhang, S., M. J. Harrison, A. T. Wittenberg, and A. Rosati, 2005: Initialization of an ENSO forecast system using a parallelized ensemble filter. *Mon. Wea. Rev.*, **133**, 3176–3201.
- Zhang, S., M. J. Harrison, A. Rosati and A. T. Wittenberg, 2007: System design and evaluation of coupled ensemble data assimilation for global oceanic climate studies. *Mon. Wea. Rev.*, **135**, 3541–3564.
- Zhang, S., A. Rosati and M. J. Harrison, 2008: Detection of multi-decadal oceanic variability within a coupled ensemble data assimilation system. *J. of Geophys. Res.*, **in press**. manuscript available at http://www.gfdl.noaa.gov/~snz/gfdl_cda2.pdf).
- Zhang, S. and A. Rosati, 2008: An ensemble circulation-dependent inflation filter in a coupled GCM – coping with deep ocean biases, Part II: Impact on oceanic climate detection. submitted to *Quart. J. Roy. Meteor. Soc.*, **Under review**.

FIGURE CAPTIONS

Fig. 1 Global mean temperature (*a*), salinity (*b*) and u-velocity (*c*) profiles produced by a 25-year time average in the last quarter of the 20th-century of 140 year CM2.0 (solid-black line, also denoted by TRUTH) and CM2.1 (dashed-black line, also denoted by CTL) historical (using temporally-varying radiative forcings) integrations, both model starting from the same coupled initial conditions at 00 UTC 1 January 1861 from previous study (Stoufer et al. 2004). The red line is produced by the ENSF’s assimilation. In the right panels, the red, green, blue lines are the annual mean RMS of temperature (*d*) and salinity (*e*) adjustments over triopical (20°S-20°N) Pacific produced by the 6-member ENSF, the 24-member ENSF and 6-member EcdiF in a 5-year (79-80) test period.

Fig. 2 Time series of the global RMS error reduction (percentage) from model control (CTL), produced by the traditional ensemble filtering biased oceanic data assimilation (ENSF) within the GFDL’s coupled data assimilation system for oceanic temperature (*a*), salinity (*b*), u-component (*c*) and v-component (*d*) of currents, and vertical motions (*e*). The “truth” is the IPCC simulation produced by CM2.0 (see section 2.1) and “observations” are produced by using the 2005 Argo network to sample the truth. Then these observations are assimilated into CM2.1 (see section 2.1) for recovering the truth. The contour interval is 5% for (*a*), (*b*), 40% for (*c*), (*d*) and (*e*).

Fig. 3 The ensemble spread of the atmosphere (upper) and the ocean (lower) in CM2.0. Each solid line (marked by a member index) represents the individual ensemble member’s departure from the ensemble mean for the last 10-year averaged global mean atmospheric/oceanic temperature (left) and atmospheric specific humidity/oceanic salinity (right) during a 25-year ensemble integration. The ensemble is initialized from 6 yearly-separate atmospheric states (including land) combining with a common oceanic state

(including sea-ice). The dotted-black lines are the standard deviation of the corresponding ensemble spread computed by the 6-member ensemble.

Fig. 4 Standard deviations of oceanic temperature (ab) and temperature and salinity correlations (T at the asterisk and S everywhere) (cd) on the x-z plane at the equator. Left panels (ac) are the results evaluated by 25-year monthly mean anomaly time series (σ_0 and ρ_0). Right panels (bd) are the 20-year time mean of 6-member ensemble-computed results ($[\sigma_t]$ and $[\rho_t]$). The contour interval is 0.02/0.002 above/below 0.01 for ab and 0.1 for cd . Note for graphing the standard deviations evaluated by the ensemble spread are multiplied by a factor of 10. The regions greater than 0.1 in ab are shaded as red and the regions greater/less than 0.4/-0.4 in cd are shaded as red/green.

Fig. 5 The time mean of $r_t(T, S)$ computed using $\kappa_t(T, S)$ (top), $r_0(T, S)$ computed by $\kappa_0(T, S)$ (middle) and their average, $r_t^{EcdiF}(T, S)$, (bottom) for the observed temperature at $140^\circ\text{W}, 0^\circ\text{N}, 2\text{ km}$, denoted by an asterisk. The contour interval is 0.04 (PSU/ $^\circ\text{C}$) and the values greater/less than 0.2/-0.2 (PSU/ $^\circ\text{C}$) are shaded as red/green.

Fig. 6 The covariance ramp function that is used to extend the adjustment amount at the bottom (2 km) of Argo profiles for $a_b^v = 1\text{ km}$ (dotted), $a_b^v = 2\text{ km}$ (dashed) and $a_b^v = 4\text{ km}$ (solid).

Fig. 7 Time series of global RMS errors at different layer (averaged) of oceanic temperature (left) and salinity (right) produced by the model control (CTL, black-dotted lines), the traditional ensemble filter (ENSF, black-solid lines), EcdiF with $Z_0 = 1\text{ km}$ and $a_b^v = a_b^{v, ENSF}$ (EcdiF₀, green-dashed lines), EcdiF with $Z_0 = 1\text{ km}$ and $a_b^v = 2a_b^{v, ENSF}$ (EcdiF₁, green-dotted lines), EcdiF with $Z_0 = 500\text{ m}$ and $a_b^v = 2a_b^{v, ENSF}$ (EcdiF₂, blue-dashed lines), EcdiF with $Z_0 = 500\text{ m}$ and $a_b^v = 4a_b^{v, ENSF}$ (EcdiF₃, blue-dashed-dotted lines) and EcdiF with $Z_0 = 0$ and $a_b^v = 4a_b^{v, ENSF}$ (EcdiF₄, red-solid lines), within one month test experiments.

Fig. 8 The horizontal distribution of the monthly-mean temperature (left) and salinity (right) adjustment amount averaged over top 500 m in EcdiF₃ (upper panels *ab*) and EcdiF₄ (lower panels *cd*) in one-month test experiment. Contour interval is 0.004 ($^{\circ}C/10^{-1}PSU$) for *ac/bd*. The regions greater/less than 0.01/-0.01 ($^{\circ}C/10^{-1}PSU$) are shaded as red/green.

Fig. 9 Time series of the global RMS error reduction (percentage) from the traditional ensemble filter (ENSF), produced by the ensemble circulation-dependent inflation filtering (EcdiF) oceanic data assimilation (EcdiF) within the GFDL’s coupled data assimilation system for oceanic temperature (a), salinity (b), u-component (c) and v-component (d) of currents, and vertical motions (e). The contour interval is 5% for (a), (b), 10% for (c), (d) and (e).

Fig. 10 The 20-year time mean (1981-2000) of global oceanic temperature (left, *ac*) and salinity (right, *bd*) errors averaged over top 2km produced by the traditional ensemble filter (ENSF) (top, *ab*) and the ensemble circulation-dependent inflation filter (EcdiF) (middle, *cd*). The corresponding “true” distributions of temperature and salinity are plotted in bottom panels as reference. The contour interval is $0.05^{\circ}C$ for *ac*, 0.02PSU for *bd*, and $0.5^{\circ}C$ for *e*, 0.1PSU for *f*.

Fig. 11 The 20-year time mean (1981-2000) assimilation errors of u-component (left) and vertical motions (right) on the x-z plane at the equator produced by ENSF (*ab*) and EcdiF (*cd*). The contour interval is 0.04 m/s for *ac*, 0.5 m/day for *bd*.

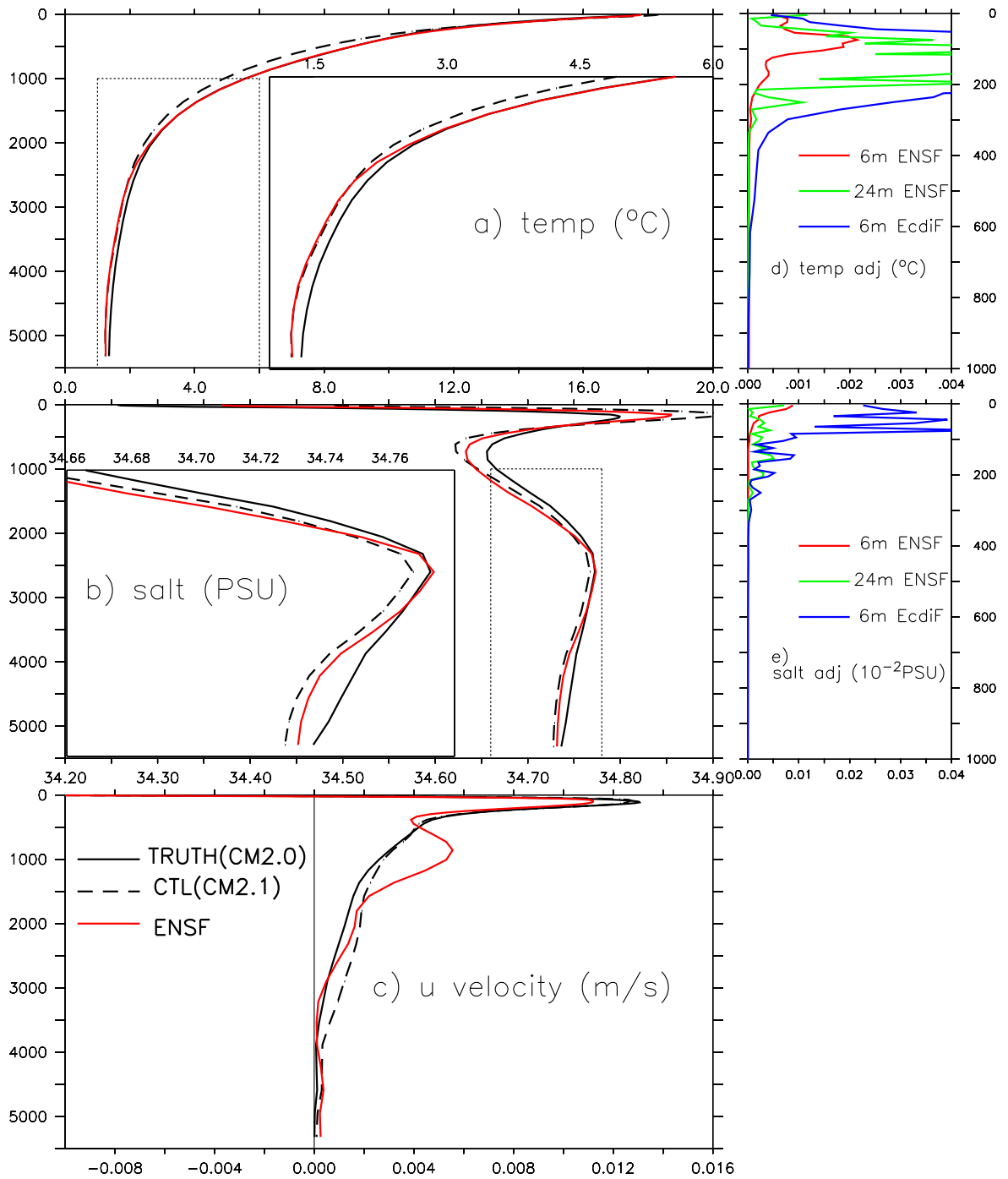


Figure 1: Global mean temperature (a), salinity (b) and u-velocity (c) profiles produced by a 25-year time average in the last quarter of the 20th-century of 140 year CM2.0 (solid-black line, also denoted by TRUTH) and CM2.1 (dashed-black line, also denoted by CTL) historical (using temporally-varying radiative forcings) integrations, both model starting from the same coupled initial conditions at 00 UTC 1 January 1861 from previous study (Stoufer et al. 2004). The red line is produced by the ENSF's assimilation. In the right panels, the red, green, blue lines are the annual mean RMS of temperature (d) and salinity (e) adjustments over tropical (20°S-20°N) Pacific produced by the 6-member ENSF, the 24-member ENSF and 6-member EcdiF in a 5-year (79-80) test period.

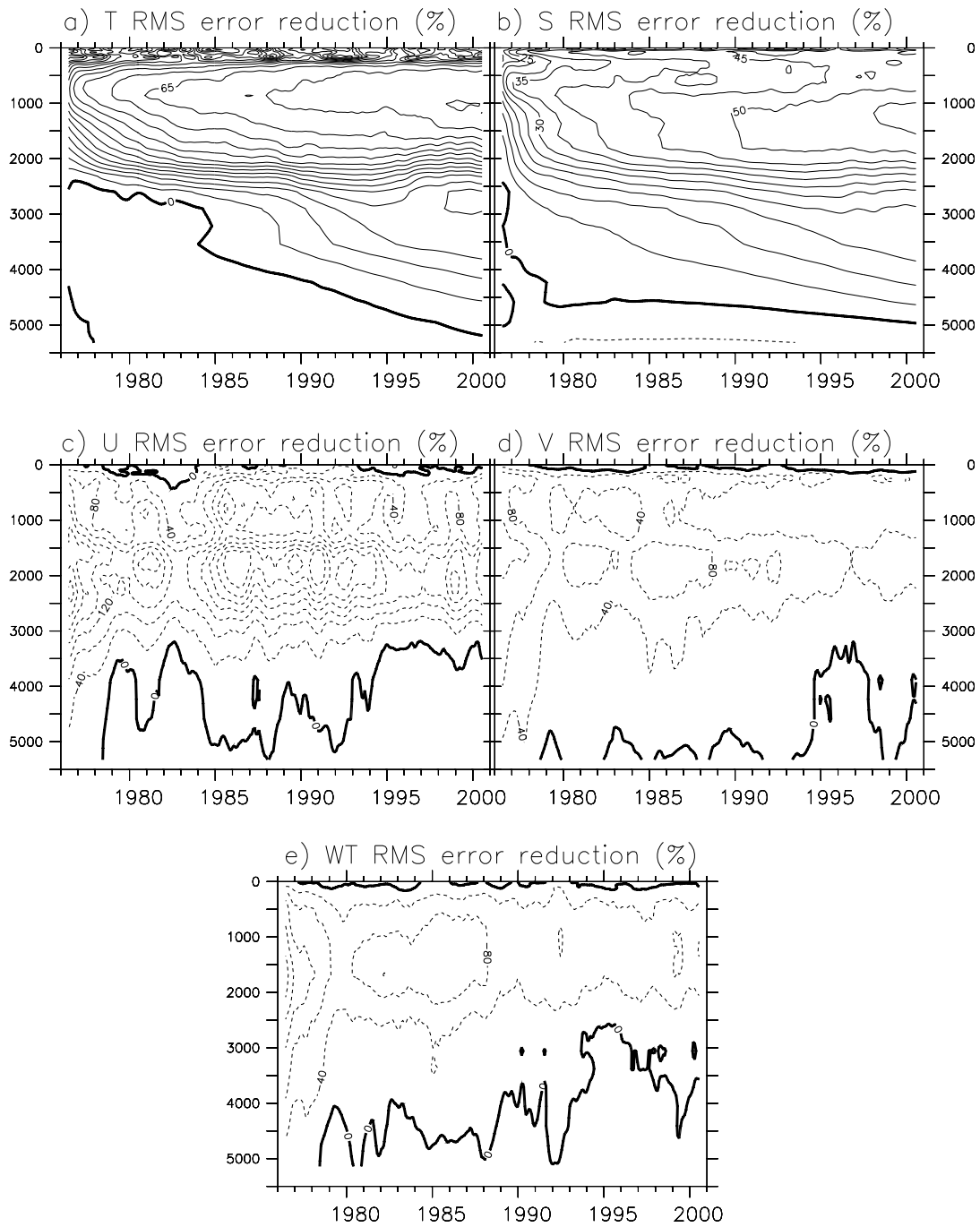


Figure 2: Time series of the global RMS error reduction (percentage) from model control (CTL), produced by the traditional ensemble filtering biased oceanic data assimilation (ENSF) within the GFDL’s coupled data assimilation system for oceanic temperature (a), salinity (b), u-component (c) and v-component (d) of currents, and vertical motions (e). The “truth” is the IPCC simulation produced by CM2.0 (see section 2.1) and “observations” are produced by using the 2005 Argo network to sample the truth. Then these observations are assimilated into CM2.1 (see section 2.1) for recovering the truth. The contour interval is 5% for (a), (b), 40% for (c), (d) and (e). A 10-month running smooth is applied for graphing.

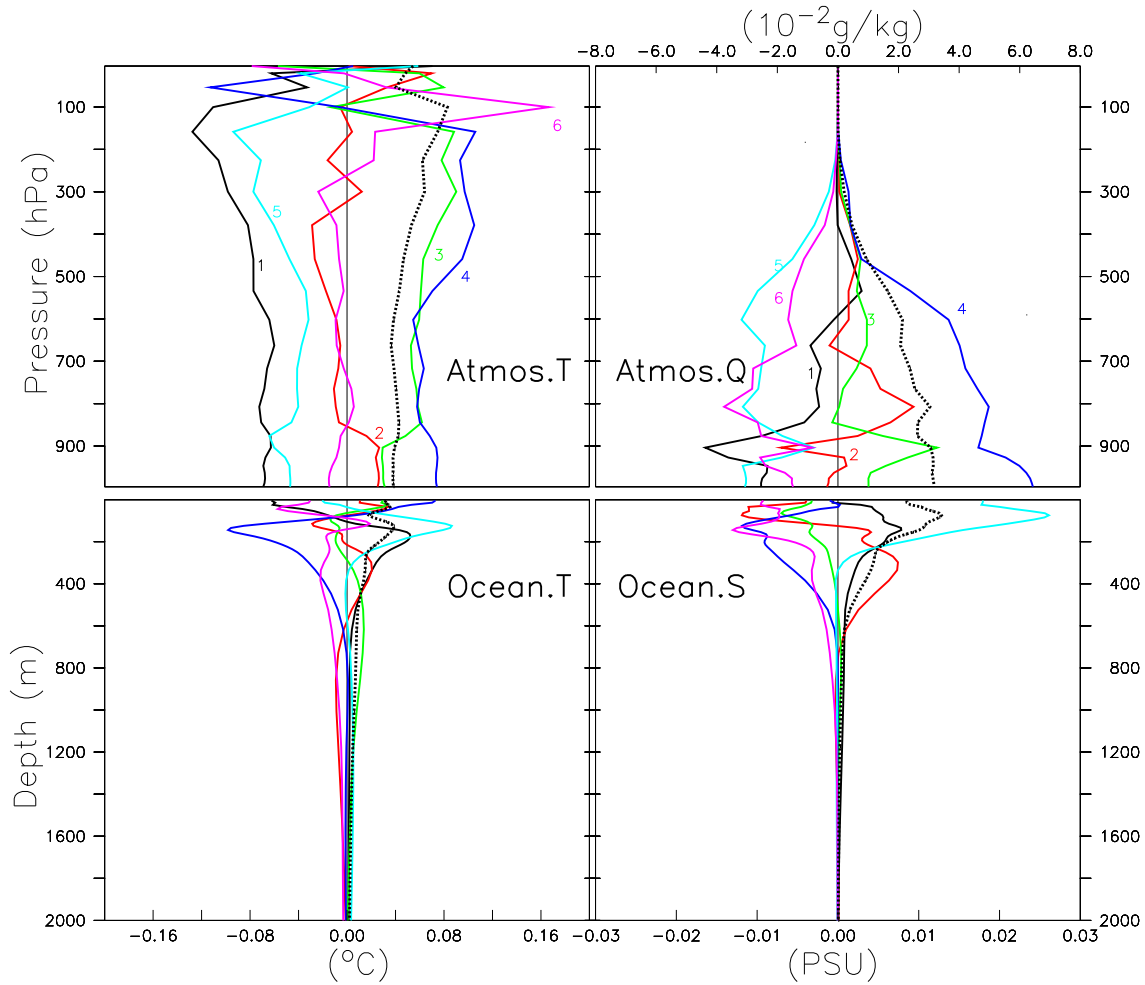


Figure 3: The ensemble spread of the atmosphere (upper) and the ocean (lower) in CM2.0. Each solid line (marked by a member index) represents the individual ensemble member's departure from the ensemble mean for the last 10-year averaged global mean atmospheric/oceanic temperature (left) and atmospheric specific humidity/oceanic salinity (right) during a 25-year ensemble integration. The ensemble is initialized from 6 yearly-separate atmospheric states (including land) combining with a common oceanic state (including sea-ice). The dotted-black lines are the standard deviation of the corresponding ensemble spread computed by the 6-member ensemble.

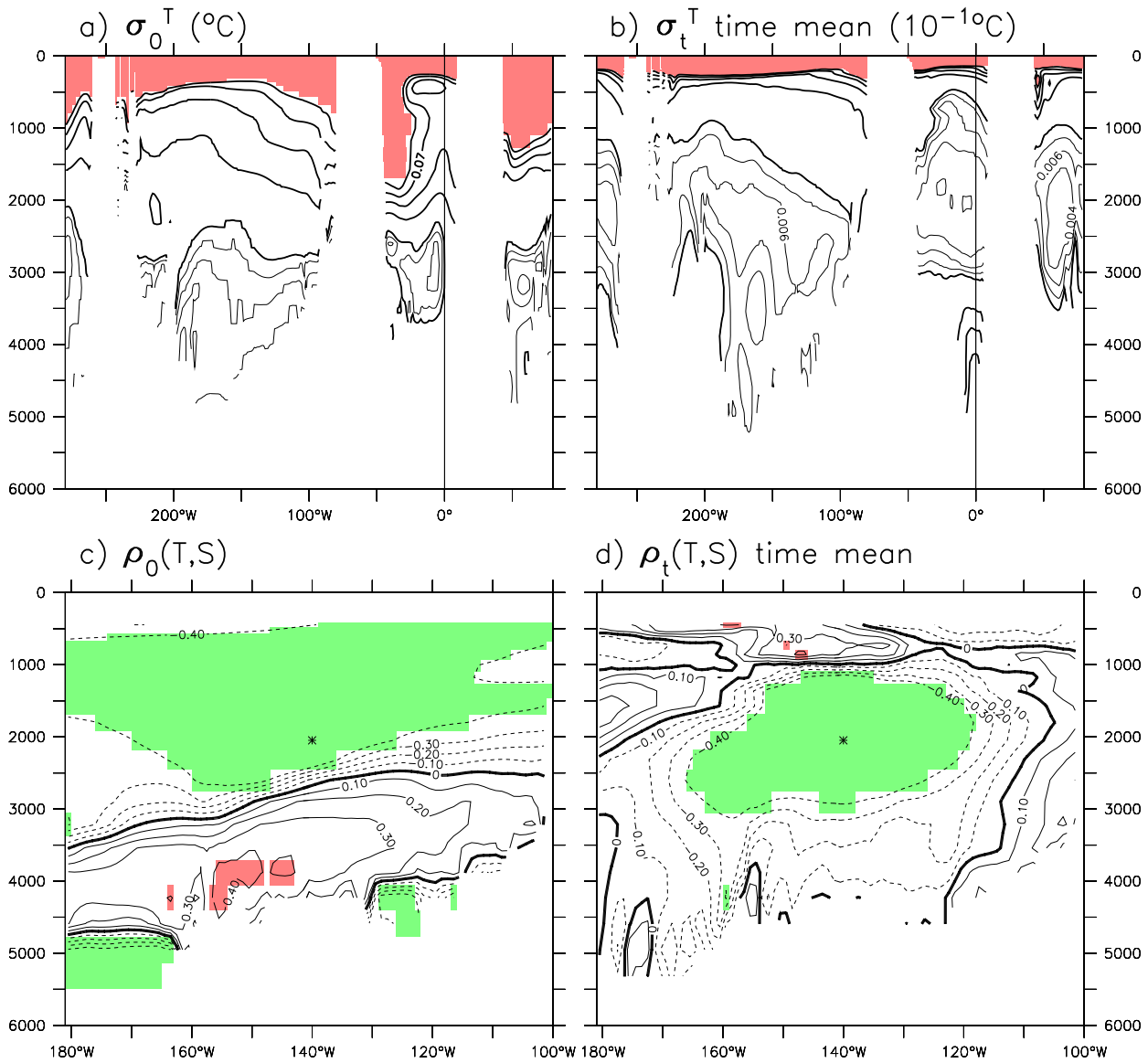


Figure 4: Standard deviations of oceanic temperature (*ab*) and temperature and salinity correlations (T at the asterisk and S everywhere) (*cd*) on the x-z plane at the equator. Left panels (*ac*) are the results evaluated by 25-year monthly mean anomaly time series (σ_0 and ρ_0). Right panels (*bd*) are the 20-year time mean of 6-member ensemble-computed results ($[\sigma_t]$ and $[\rho_t]$). The contour interval is 0.02/0.002 above/below 0.01 for *ab* and 0.1 for *cd*. Note for graphing the standard deviations evaluated by the ensemble spread are multiplied by a factor of 10. The regions greater than 0.1 in *ab* are shaded as red and the regions greater/less than 0.4/-0.4 in *cd* are shaded as red/green.

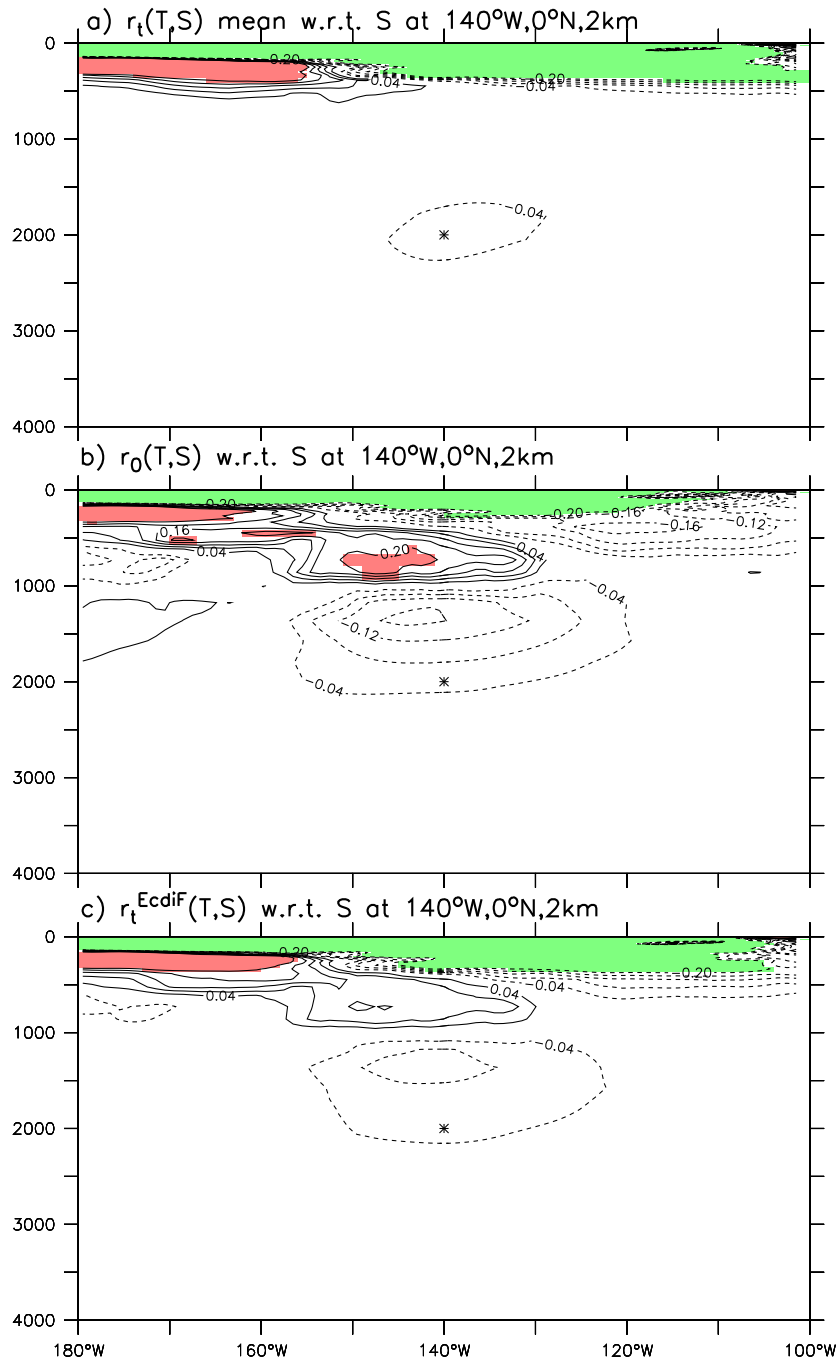


Figure 5: The time mean of $r_t(T, S)$ computed using $\kappa_t(T, S)$ (top), $r_0(T, S)$ computed by $\kappa_0(T, S)$ (middle) and their average, $r_t^{\text{EcdiF}}(T, S)$, (bottom) for the observed temperature at $140^\circ\text{W}, 0^\circ\text{N}, 2\text{ km}$, denoted by an asterisk. The contour interval is 0.04 ($\text{PSU}/^\circ\text{C}$) and the values greater/less than $0.2/-0.2$ ($\text{PSU}/^\circ\text{C}$) are shaded as red/green.

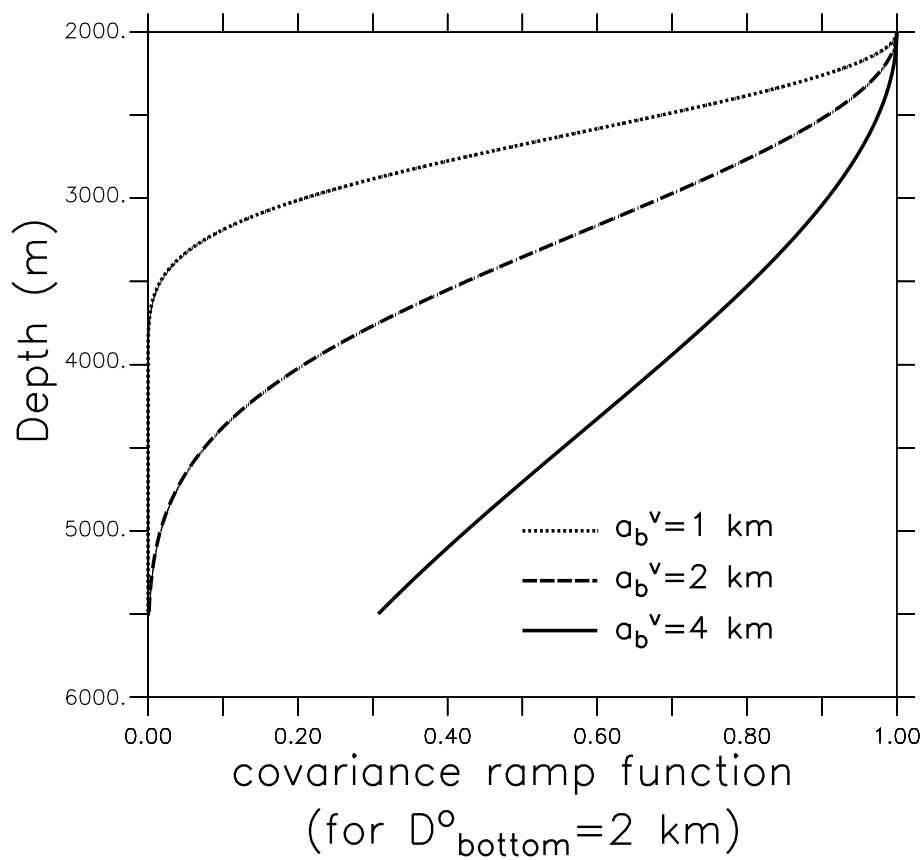


Figure 6: The covariance ramp function that is used to extend the adjustment amount at the bottom (2 km) of Argo profiles for $a_b^v = 1$ km (dotted), $a_b^v = 2$ km (dashed) and $a_b^v = 4$ km (solid).

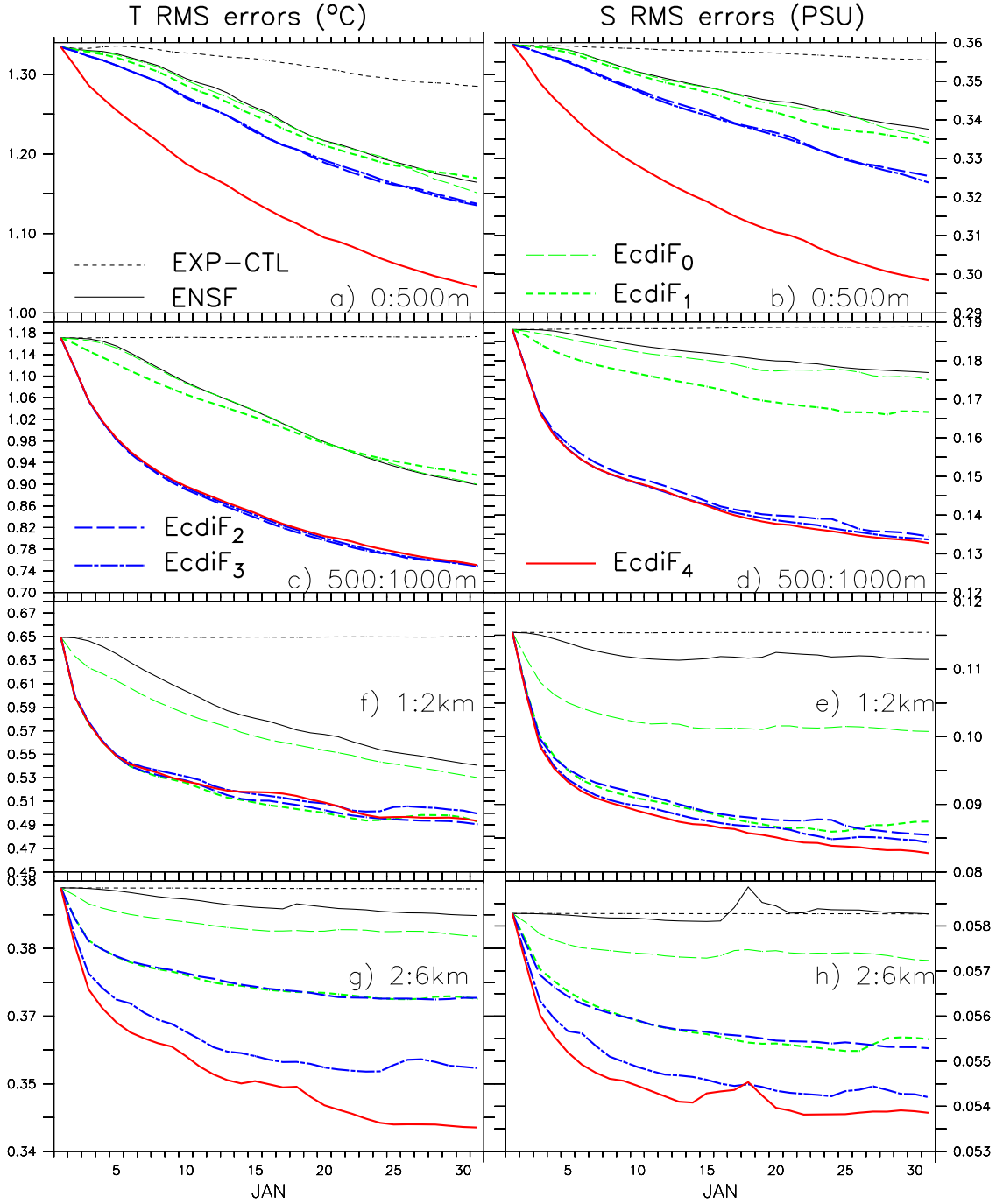


Figure 7: Time series of global RMS errors at different layer (averaged) of oceanic temperature (left) and salinity (right) produced by the model control (CTL, black-dotted lines), the traditional ensemble filter (ENSF, black-solid lines), EcdiF with $Z_0 = 1$ km and $a_b^v = a_b^{v,ENSF}$ (EcdiF₀, green-dashed lines), EcdiF with $Z_0 = 1$ km and $a_b^v = 2a_b^{v,ENSF}$ (EcdiF₁, green-dotted lines), EcdiF with $Z_0 = 500$ m and $a_b^v = 2a_b^{v,ENSF}$ (EcdiF₂, blue-dashed lines), EcdiF with $Z_0 = 500$ m and $a_b^v = 4a_b^{v,ENSF}$ (EcdiF₃, blue-dashed-dotted lines) and EcdiF with $Z_0 = 0$ and $a_b^v = 4a_b^{v,ENSF}$ (EcdiF₄, red-solid lines), within one month test experiments.

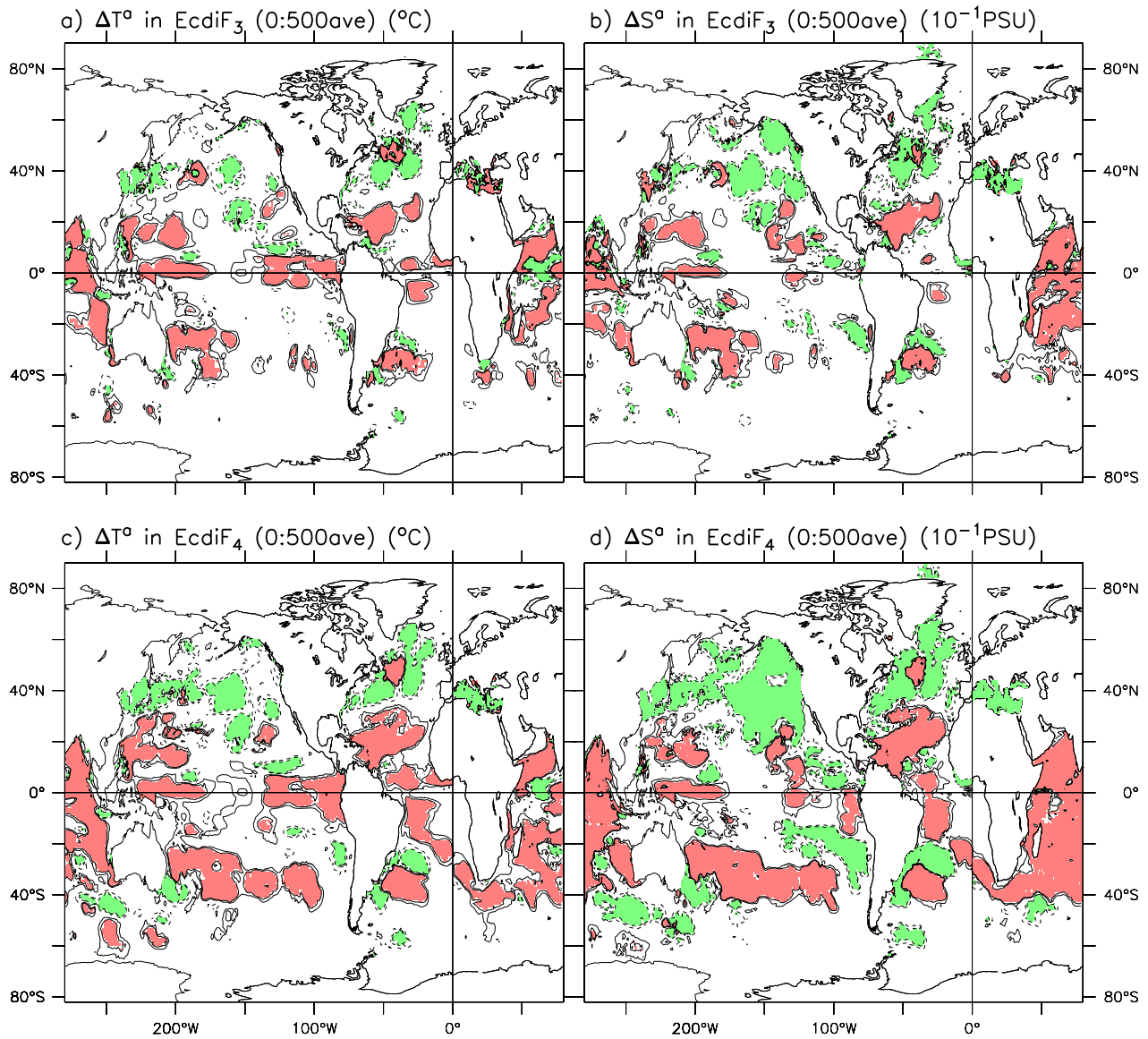


Figure 8: The horizontal distribution of the monthly-mean temperature (left) and salinity (right) adjustment amount averaged over top 500 m in EcdiF₃ (upper panels *ab*) and EcdiF₄ (lower panels *cd*) in one-month test experiment. Contour interval is 0.004 (°C/10⁻¹PSU) for *ac/bd*. The regions greater/less than 0.01/-0.01 (°C/10⁻¹PSU) are shaded as red/green.

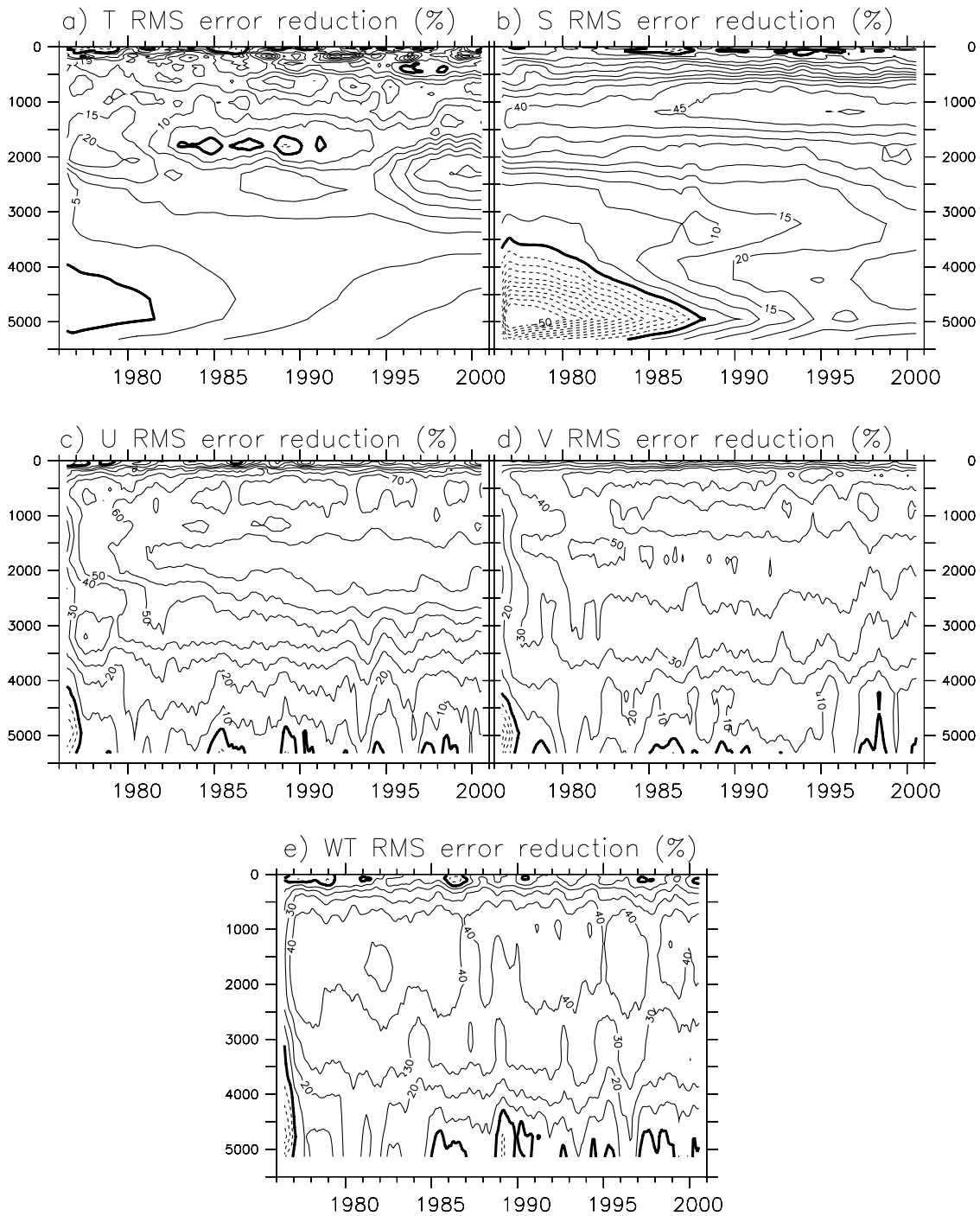


Figure 9: Time series of the global RMS error reduction (percentage) from the traditional ensemble filter (ENSF), produced by the ensemble circulation-dependent inflation filtering oceanic data assimilation (EcdiF) within the GFDL's coupled data assimilation system for oceanic temperature (a), salinity (b), u-component (c) and v-component (d) of currents, and vertical motions (e). The contour interval is 5% for (a), (b), 10% for (c), (d) and (e). A 10-month running smooth is applied for graphing.

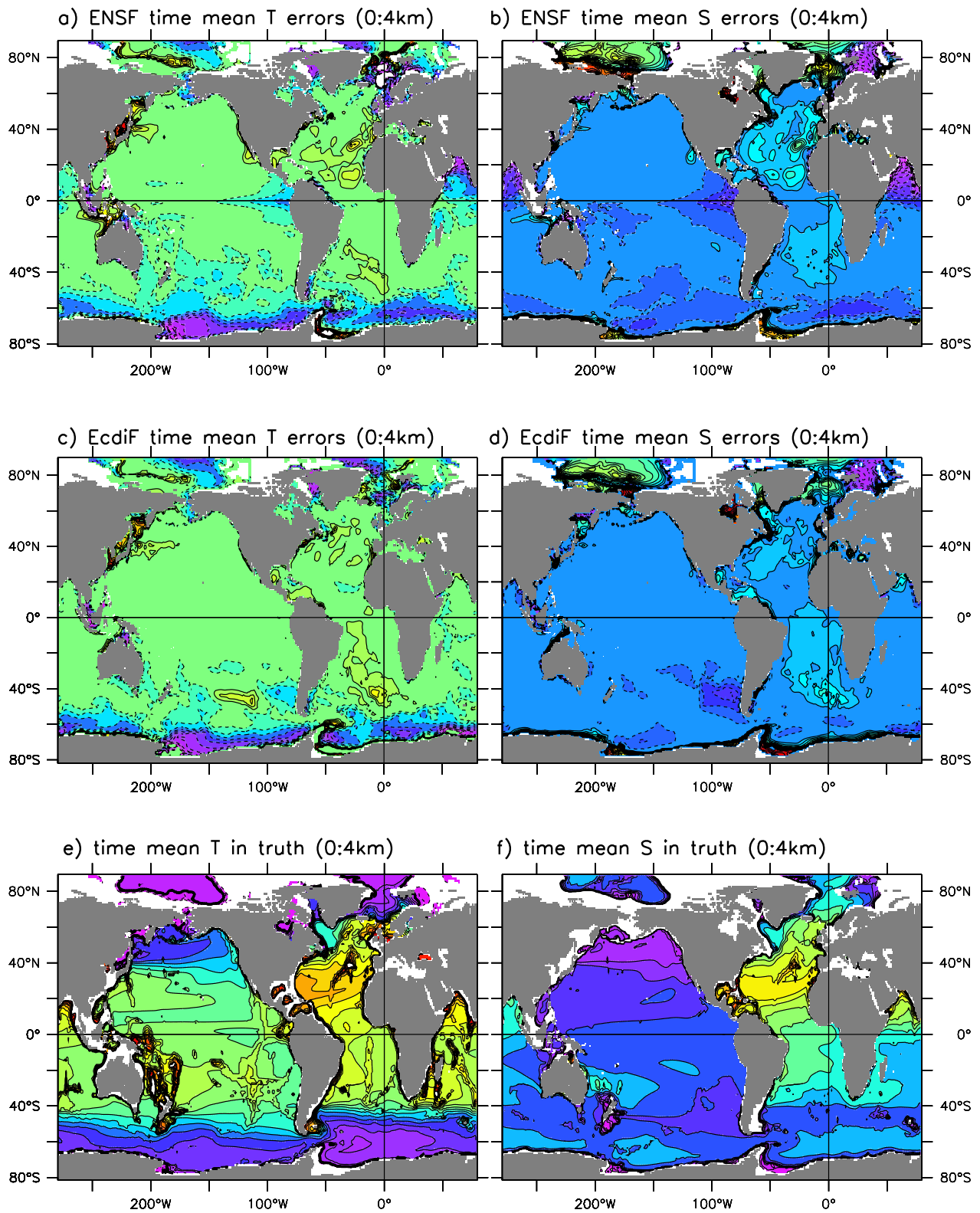


Figure 10: The 20-year time mean (1981-2000) of global oceanic temperature (left, *ac*) and salinity (right, *bd*) errors averaged over top 4km produced by the traditional ensemble filter (ENSF) (top, *ab*) and the ensemble circulation-dependent inflation filter (EcdiF) (middle, *cd*). The corresponding “true” distributions of temperature and salinity are plotted in bottom panels as reference. The contour interval is 0.05°C for *ac*, 0.02PSU for *bd*, and 0.5°C for *e*, 0.1PSU for *f*.

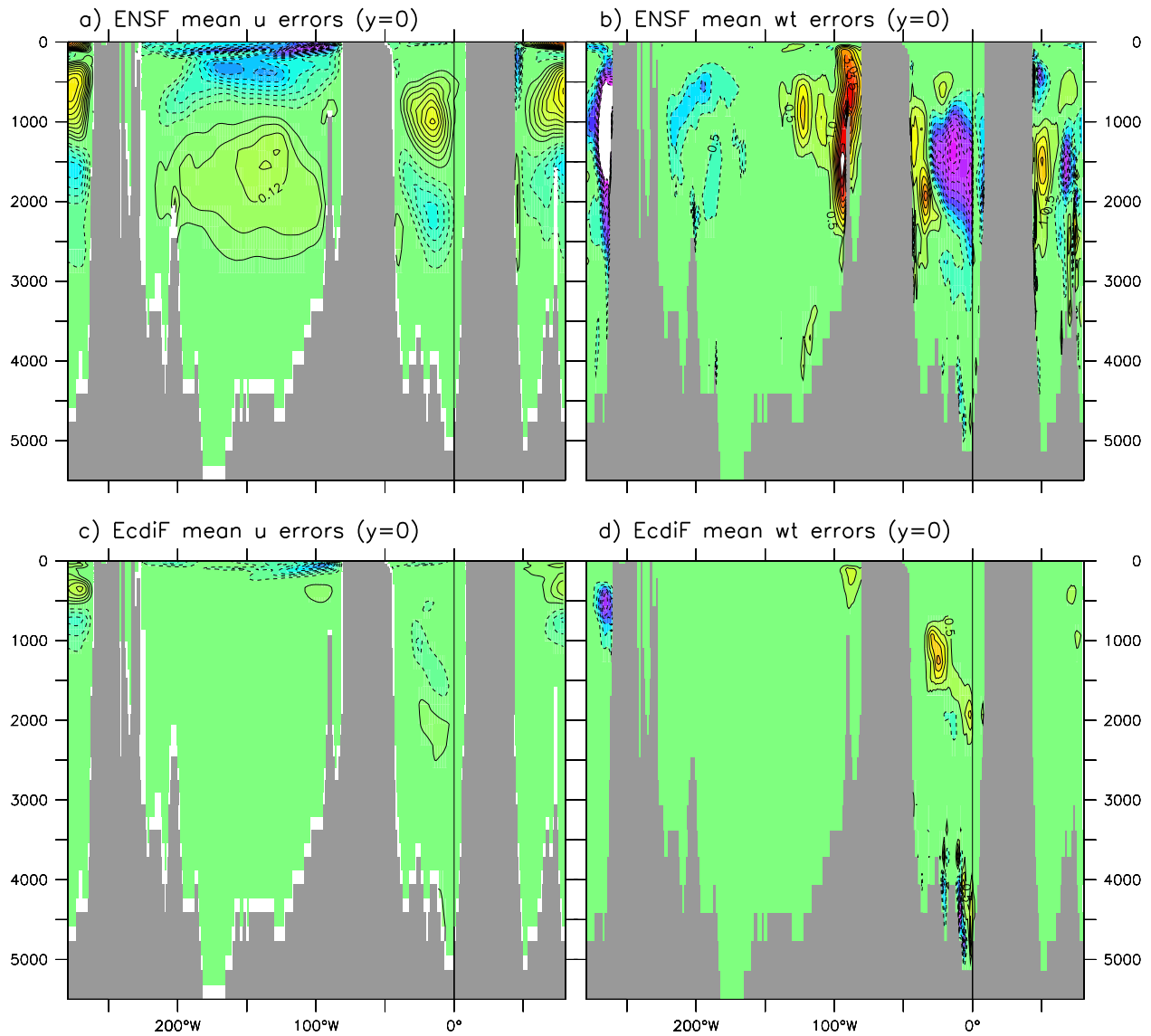


Figure 11: The 20-year time mean (1981-2000) assimilation errors of u-component (left) and vertical motions (right) on the x-z plane at the equator produced by ENSF (*ab*) and EcdiF (*cd*). The contour interval is 0.04 m/s for *ac*, 0.5 m/day for *bd*.